CHALMERS

Assessment of cast-in-situ FRC linings for high-speed railway tunnels with respect to fatigue and cracking

Final Report – project number TRV 2017/110859

CARLOS GIL BERROCAL
INGEMAR LÖFGREN
KARIN LUNDGREN

Department of Architecture and Civil Engineering
Division of Structural Engineering
Concrete Structures
CHALMERS UNIVERSITY OF TECHNOLOGY
Göteborg, Sweden 2018

Assessment of cast-in-situ FRC linings for high-speed railway tunnels with respect to fatigue and cracking

Final Report – project number TRV 2017/110859

Department of Architecture and Civil Engineering
Division of Structural Engineering
Concrete Structures
CHALMERS UNIVERSITY OF TECHNOLOGY
Göteborg, Sweden 2018

Assessment of cast-in-situ FRC linings for high-speed railway tunnels with respect to fatigue and cracking - Final Report – project number TRV 2017/110859

CARLOS GIL BERROCAL
INGEMAR LÖFGREN
KARIN LUNDGREN

2018
Chalmers Tekniska Högskola

Department of Architecture and Civil Engineering
Division of Structural Engineering
Concrete *Structures*
Chalmers University of Technology
SE-412 96 Göteborg
Sweden
Telephone: + 46 (0)31-772 1000

Cover: [*Insert description of the cover image*]

Contents

Summary

This report presents the results of a pre-study aimed at investigating a number of critical aspects identified for the execution of a fibre reinforced concrete lining in relation to the construction of high-speed railways in Sweden. The work carried out focused primarily on the study of fatigue performance of FRC and on the structural response of the tunnel lining under the actions of various loads including air pressure and suction, shrinkage and temperature changes.

In the first part of the report a literature review was carried out to examine the state-of-the-art of fatigue of FRC and derive some qualitative relations to evaluate the risk of fatigue failure due to cyclic loading of the tunnel lining (10^6 cycles). Subsequently, the tunnel lining was modelled using the commercial finite element software DIANA and non-linear analyses were carried out to determine the risk of cracking and the potential crack widths for a number of load cases.

The main results of this pre-study showed that fibres can provide a small enhancement of the fatigue performance of FRC compared to plain concrete for moderate fibre dosages of up to 1.0% vol. Nevertheless, the effect of reverse loading and existing cracks on the fatigue behaviour of FRC are largely unexplored and require further investigation. It was also found that cyclic loading due to the air pressure and suction from passing trains produced a maximum stress variation of about 10% of the concrete tensile strength, thus posing no risk for fatigue failure provided the concrete lining is uncracked. Conversely, non-uniform shrinkage and temperature gradients were able to induce cracking. In cracked conditions, the air pressure and suction were sufficient to produce excessively large cracks, thereby posing a risk for the fatigue life and durability of the tunnel.

Preface

The work presented in this report was carried out within a research pre-study funded by Trafikverket entitled "*Förstudie Fiberarmerad dränerad betonglining i tunnlar för höghastighetståg*" with reference number TRV 2017/110859. The work was carried out at the Concrete Structures research group, division of Structural Engineering at Chalmers University of Technology, between February and November of 2018 by Dr. Carlos Gil Berrocal, Adj. Professor Ingemar Löfgren and Professor Karin Lundgren.

A reference group was formed to provide inputs and feedback and to discuss the findings of the project. The members of the reference group included Kurt Palmqvist, Olle Olofsson and Karl-Johan Loorents from Trafikverket as well as Anders Fredriksson acting as an independent consultant.

Göteborg, December 2018

Carlos Gil Berrocal

1 Introduction

1.1 General background

In Sweden, the use of concrete lining (cast-in-place tunnel lining) in rock tunnels has been very limited with few exceptions. The main reason can be attributed to the favourable conditions in the rock where a strengthening system combining rock bolts and sprayed concrete is usually sufficient. Nevertheless, tunnels designed to enable the traffic of high-speed trains require higher demands. Examples of tunnels with concrete lining can be readily found in many countries.

For the construction of the high-speed railway project (Göteborg – Borås and Ostlänken), Trafikverket has preliminary projected a number of tunnels in rock with an inner concrete lining. One of the options considered for the execution of the lining is to use fibre reinforced concrete.

The advantage of using fibre reinforced concrete for the construction of the tunnel lining is a significantly easier and shorter construction process. As a result, fibre reinforced concrete has been increasingly used in tunnel linings during the last years, particularly in the form of precast tunnel lining segments (segmental lining) which are often used for tunnels executed with TMB (tunnel boring machine). Examples of projects where segmental lining has been used are the Channel Tunnel Rail Link (UK), the Oenzberg tunnel between Zurich and Bern (Switzerland) and the Metro in Barcelona (Spain), to mention a few. Moreover, in the beginning of the 1990's, design methods and techniques were developed in Japan for extruded fibre reinforced concrete linings [1,2].

The tunnel lining projected by Trafikverket has been analysed in previous studies, the results of which can be found in two reports:

1) "Inner Lining – Verification for the tunnel (double track) section", Studies on Inner Lining v03 from Amberg Engineering AG and Bergab.

2) "PM – Analys av dränerad betonglining för dubbelspårstunnel", by Anders Fredriksson.

In the first report, both an unreinforced and a fibre reinforced concrete lining were analysed. The computer software Sofistik was used to model the tunnel lining using beam elements while the mechanical properties of the fibre reinforced concrete were defined according to the DAfStb Richtlinie Stahlfaserbeton [3]. The conclusion in that report was that a 500 mm thick unreinforced concrete lining or a 300 mm fibre reinforced concrete lining fulfill the load bearing requirements. However, fatigue was not considered in the calculations and the resulting crack width, which was found to be between 0.4 and 0.6 mm in Serviceability Limit State (SLS), was estimated based on simplified assumptions.

In the report "Analys av dränerad betonglining för dubbelspårstunnel", the computer software PLAXIS 2D was used and the stresses with regard to fatigue were checked according to BBK 04. The conclusion was that a 300 mm thick tunnel lining was not enough to fulfill the fatigue requirements without reinforcement. However, fatigue was not investigated for the fibre reinforced concrete alternative.

In connection with the results presented in the aforementioned reports, several aspects requiring further research were identified. One aspect that needs to be highlighted and further investigated is the impact of cyclic loading caused by air pressure (suction and pressure) generated when the trains pass through the tunnel. This is of particular interest for fibre reinforced concrete, since fibre concrete is not currently treated in Eurocode 2 (SS-EN 1992-1 & EN 1992-2). Fatigue is not considered either in the available recommendations for the design of fibre reinforced concrete, such as the Model Code 2010 [4] or the DAfStb Richtlinie Stahlfaserbeton [3]. However, a significant amount of literature exists concerning the study of the fatigue of fibre reinforced concrete, see e.g. [5–7], which can form the basis of the investigation work to be carried out.

Other important aspects that were also identified include the loads to be applied on the concrete lining and the effect of the chosen static system. This concerns especially the risk of restraint cracking in the tunnel lining arising from temperature variations, which were found to be a limiting factor for the design of the lining in the first report. Accordingly, the analysis of crack widths and crack heights was also deemed crucial to ensure the functionality and durability of the fibre reinforced concrete lining. Further relevant aspects for the design of the lining that were not addressed in the present study include the load effect arising from ice formation at the interface between the lining and the rock bed caused by the presence of sub-zero temperatures in the rock. An estimation of the risk to reach sub-zero temperature in the rock was nevertheless performed.

1.2 Purpose and objectives

The main purpose of this pre-study was to investigate some of the aspects requiring further research that were identified in the previous reports to assess the viability of using a 300 mm thick fibre reinforced concrete inner lining for the construction of a high-speed railway project. Consequently, the objectives of this pre-study are the following:

- Create a finite element model to enable non-linear structural analysis of the tunnel including the concrete cracking due to the external loads.
- Determine the stress variation and bearing capacity of the tunnel lining under cyclic loading caused by air pressure and suction.
- Study the influence of the number of cycles and the stress range on the fatigue behaviour of fibre reinforced concrete (uncracked and cracked section).
- Estimate the expected air temperature in the tunnel based on available historic temperature data and temperature difference measurements.
- Determine the temperature variation in the tunnel lining based on the thermal properties of the concrete and rock material as well as the expected air temperature inside the tunnel.
- Determine the effect of the temperature variations on the restraint cracking.

1.3 Methodology

The work carried out within this pre-study can be divided into three main parts: (i) a review study on fatigue of fibre reinforced concrete, (ii) an evaluation of the environmental conditions inside the tunnel lining and (iii) the structural assessment of the tunnel lining.

In the first part, our efforts were devoted to compile, analyse and compare existing knowledge and experience on the characterization of fatigue strength of fibre reinforced

cementitious composites. The next part of the pre-study involved the determination of the environmental conditions in terms of temperature and relative humidity that might be expected inside of the tunnel. Finally, the last part involved the modelling and analysis of the tunnel lining using the commercial finite element software DIANA, which enables non-linear analysis of concrete elements thereby allowing the modelling of concrete cracking and the estimation of the resulting crack widths.

1.4 Reference documents for the basis of structural design

The actions required for the structural analysis of the tunnel lining are taken according to the specifications of the report "TRVK Tunnel 11 – *Trafikverkets tekniska krav Tunnel*" published by Trafikverket [8], which include:

(a) The magnitude of the load to be applied on the inner side of the tunnel lining to simulate the air pressure / suction generated during the passing of trains.
(b) The number of loading cycles to be resisted by the tunnel lining.
(c) The temperature variation to be applied during the period of summer and winter, respectively.

The geometry of the cross-section of the double-track tunnel lining as well as the parameters defining the stiffness of the contact between the lining and the rock bed were obtained from first pre-study "Inner Lining – Verification for the tunnel (double track) section". Similarly, the mechanical properties defining the strength and post-cracking behavior of the fibre reinforced concrete were adopted from the same document, which in turn are defined in accordance to the German design guidelines DAfStb Richtlinie Stahlfaserbeton.

The information needed to perform the heat transfer analyses in terms of the thermal properties of the concrete and rock materials were extracted from the second pre-study report "PM – Analys av dränerad betonglining för dubbelspårstunnel".

Last, data regarding temperature measurements inside and outside existing tunnels of similar characteristics to the one under study were obtained from the report "Förstudie: Temperaturer i höghastighetsbarnorna tunnlar" by EQUA.

1.5 Outline of the report

The report is divided into five chapters describing the main findings of the pre-study.

Chapter 1 describes the background, motivation and purpose of the pre-study as well as the objectives, methodology and outline of the report.

In Chapter 2, a summary of the available research results regarding fatigue of fibre reinforced concrete is presented, together with a comparison between the fatigue behaviour of plain concrete and fibre reinforced concrete.

Chapter 3 outlines the procedure and data used to estimate the expectable average environmental conditions inside of the tunnel in terms of temperature and relative humidity.

In Chapter 4, the implementation of the finite element model is described as well as the parameters used for the numerical analyses, including a 1D moisture transport analysis, a 1D heat transfer analysis and a 2D structural analysis of the concrete lining.

Chapter 5 summarizes the main findings of the pre-study and includes the concluding remarks.

2 Review of fatigue of fibre reinforced concrete

Fatigue is regarded as a critical aspect for the design of structures subjected to repeated loading because it may lead to structural failure even when the loads acting on the structure are below the design loads. Consequently, for structures or structural elements subjected to cyclic loading, it is imperative to be aware of the fatigue behaviour of the constitutive materials and design the structures accordingly.

The aim of this chapter is to is to provide a qualitative description of the fatigue behaviour of fibre reinforced concrete and how it compares to plain concrete. This has been accomplished by reviewing the existing literature reporting experimental results of fatigue tests in FRC. The review includes some of the most recently published studies as well as studies that date back to up to more than four decades ago.

2.1 General background

Fatigue is often described as the progressive and non-reversible internal damage process that materials experience under the action of cyclic loading. In concrete, this damage can be mainly attributed to the initiation and gradual growth of internal micro-cracks that progressively coalesce into macro-cracks. These macro-cracks lead to changes in the mechanical and transport properties of the material at the structural scale, such as a reduction of stiffness or an increase of permeability. Eventually, the crack growth rate increases sharply causing the failure of the loaded element.

Regarding fatigue loading, two different types are usually differentiated: low-cycle loading, which involves a low number of loading cycles at high stress levels, such as seismic events, and high-cycle loading involving a large number of cycles at lower stress levels, e.g. due to traffic, wind or sea waves loading.

The most common approach to study and assess the fatigue life of structural elements is the use of empirically derived S-N diagrams, also known as Whöler curves. In these empirical curves, the stress range or stress amplitude of the cyclic loading is presented as a function of the number of cycles that the material is able to withstand, in logarithmic scale. As such, this approach gives a clear graphical representation of the fatigue performance which may also include the effect of other loading parameters such as the mean stress. However, fatigue is a very complex phenomenon that depends on multiple parameters including the loading and boundary conditions, loading frequency, stress range and maximum stress ratio.

Moreover, due to added complexity arising from the composite nature of cement-based materials, the understanding of the fatigue behaviour of concrete is lagging behind that of metals like steel. Furthermore, the inclusion of fibre reinforcement into the matrix further increases the complexity of the mechanisms controlling the fatigue of concrete by adding the effect of parameters related to the fibres themselves. Subsequently, the knowledge gap becomes even more evident in the case of FRC. For instance, the existence of an endurance limit, i.e. a stress range below which the material can endure an infinite number of loading cycles, which is observed in metals but not in plain concrete, is one of the aspects that is still debated for FRC.

2.2 Comparison of reviewed studies

The lack of understanding and consensus among researchers is the main reason for the current absence of guidelines and recommendations for the design of FRC members with regard to fatigue. Similarly, there is currently no standard procedure for testing of

Table 1. Summary of reviewed research studies regarding fatigue of steel fibre reinforced concrete

Reference	Type of test	Specimen			Material		Loading	
		Shape	Dimensions [mm]	Pre-cracked	Concrete strength [MPa]	Fibre dosage [% vol.]	Stress range [% of f_c /f_{ct}] /f_{cfl}]	Frequency [Hz]
Batson et al. 1972 [9]	3-point bending	Beams	101×152×258	No	35	2 – 2.98	95-92-85-79-66	3
Otter et al. 1988 [10]	Uniaxial compression	Cylinders	Ø100×200	No	25	1-2-3	90	n/a
Johnston et al. 1991 [6]	3-point bending	Beams	102×102×356	No	n/a	0.5-1-1.5	99-95-90-85-80-75	n/a
Nanni et al. 1991 [11]	4-point bending	Beams	102×102×356	No	41.5	0.46	95-90-85-80-75	20
Grzywoski et al. 1993 [12]	Uniaxial tension	Cubes	102	No	48	0.25-0.5-0-75-1	90-80-75-70	n/a
Chang et al. 1995 [13]	3-pooint bending	Beams	100×100×600	No	n/a	0.5-1-1.5-2	85-80-75-70	10
Chenkui et al. 1995 [14]	4-point bending	Beams	150×150×550	No	42.5	1-1.5-2	0.95 to 0.65	5-20
Mailhot et al. 2001 [15]	3-point bending	Beams	125×125×425	No	45	0.5	85-80-75-70-65	20
Singh et al. 2001 [16]	3-point bending	Beams	100×100×500	No	42.3	0.5-1-1.5	90-85-80-75-65	12

n/a = not available

Table 1. Summary of reviewed research studies regarding fatigue of steel fibre reinforced concrete (cont).

Reference	Type of test	Specimen			Material		Loading	
		Shape	Dimensions [mm]	Pre-cracked	Concrete strength [MPa]	Fibre dosage [% vol.]	Stress range [% of f_c /f_{cd}] /f_{cfl}]	Frequency [Hz]
Singh et al. 2006 [17]	4-point bending	Beams	100×100×500	No	65	1-1.5-2	90-85-80-70	20
Graeff et al. 2012 [18]	3-point bending	Beams	150×150×550	No	55	2	90-70-50	15
Germano et al. 2016 [7]	3-point bending	Beams	150×150×550	Yes	45	0.5-1	85-75-65	2 to 5
Goel et al. 2016 [19]	4-point bending	Beams	100×100×500	No	40	0.5-1-1.5	90-85-80-75-70	10
Banjara et al. 2016 [20]	3-point bending	Beams	100×100×500	No	48	0.5	85-75-65	5
Isojeh et al. 2017 [21]	Uniaxial tension	Dogbone	70×200×500	No	55	0.75-1.5	95-90-85-80-75	5

fatigue performance of concrete or FRC, which means that the testing procedures used in different studies may vary significantly. Table 1 presents a list of studies reporting experimental results on the fatigue behaviour of FRC, where some of the parameters from each study have been summarized including type of test, specimen geometry and dimensions, fibre dosage and stress range investigated as well as the frequency of the applied cyclic loading.

As observed, different types of test have been used to study the fatigue performance of FRC including uniaxial tension, uniaxial compression and flexural tests. The most commonly performed tests are the flexural tests although both 3-point and 4-point bending configurations as well as different specimen geometries, concrete qualities and loading conditions have been used. Based on the many differences between the testing procedures used by different researchers, it is arguable whether the FRC fatigue life results from different studies may or may not be directly compared. Nevertheless, the stress values presented in S-N diagrams are most often made dimensionless by normalizing to the concrete static strength (tensile, compressive or flexural), which partly eliminates some of the dependencies on the geometry and strength of the material.

Even though it is still not obvious whether S-N diagrams obtained from multiple tests programmes involving different loading setups and testing conditions may be directly compared, by combining the reported results of various studies into a unique diagram, additional information could be unlocked. In particular, it may be possible to discern a general trend for the fatigue behaviour of FRC as well as how FRC compares to plain concrete in terms of fatigue life. It should be noted, however, that although fibres may also have a significant impact on aspects such as the fatigue-induced crack pattern, the crack growth rate or the total strain attained before failure, in this study the comparison was focused solely on the fatigue life. Likewise, only studies incorporating steel fibres have been considered in this review.

In Figure 1(a)-(f) the compiled S-N experimental results from different studies investigating flexural fatigue are presented for plain concrete and for SFRC at several fibre dosages ranging between 0.5% vol. and 3.0% vol. Moreover, the average number of cycles resisted at a certain stress level have been highlighted and regression lines including the data points of all the combined sets, which can be later used as a reference to compare with numerical analyses results, have been added.

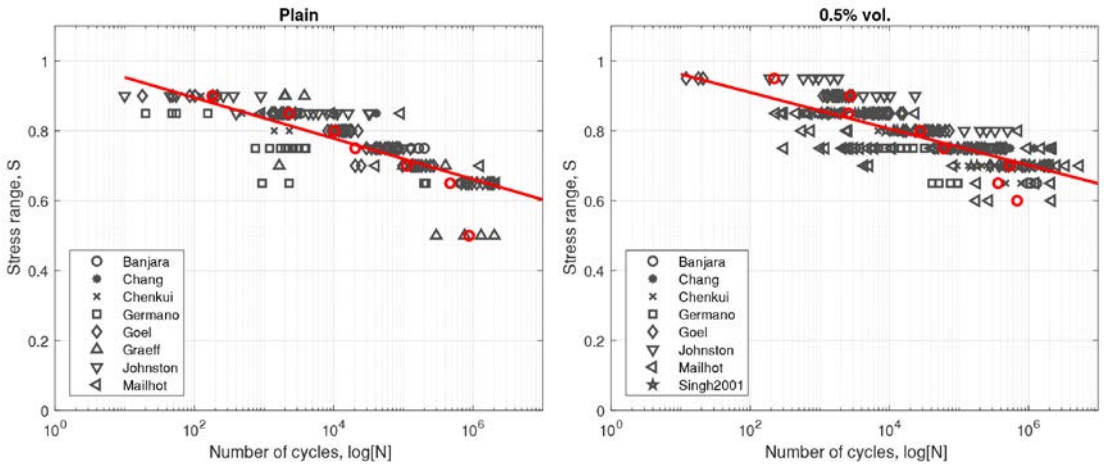

(a) (b)

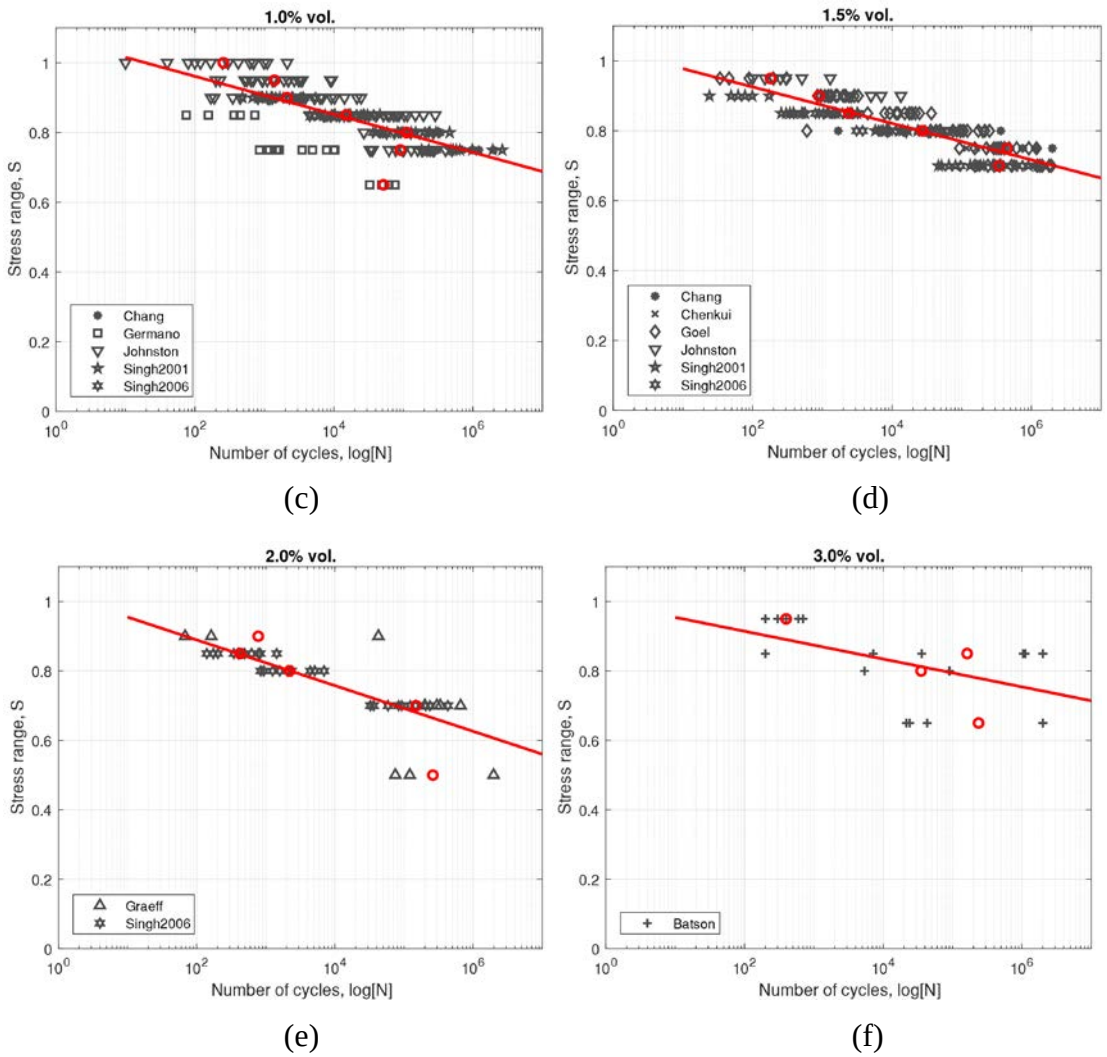

Figure 1. S-N diagrams showing the combined experimental results from flexural fatigue tests performed on plain concrete and SFRC obtained from the different studies reviewed.

From Figure 1 it can be seen that most of the studies focused on fibre dosages of up to 1.5% vol. whereas for higher fibre contents the available data is scarce and the found trends might not be relevant. For the cases where data is available from several studies, it can be observed that the scatter is significant both between different studies but also within results from individual studies. In particular, the results by Mailhot et al. [15] shown in Figure 1(b) display a very large variability where for a stress ratio of 0.75, fatigue failure was observed as soon as just a few hundred cycles and as late as more than 1 million cycles. This could be attributed to the fact that results from different mixes with different *w/c* ratios and, more importantly, with various fibre types (end-hooked, nail-anchored and crimped) featuring different aspect ratios, have been lumped together, which may indicate the importance of the fibre characteristics.

Another important observation, specifically from Figure 1(c), is that the results from Germano et al. [7] show a consistently reduced fatigue life compared to other studies. This is most likely due to the testing procedure used in their study where the specimens featured a pre-cracked state compared to the rest of studies where fatigue tests were conducted on uncracked specimens. It is also noteworthy that the difference in fatigue life between uncracked and pre-cracked specimens seems less apparent for plain concrete and low dosage FRC mixes. Nevertheless, more studies on pre-cracked specimens are needed to validate the observed trend and better quantify the impact of

existing cracks, which is a very relevant issue since fibres are most often added to concrete for crack control purposes.

In order to assess the effect of fibres based on the experimental results from the reviewed studies, the regression lines included in Figure 1 have been plotted separately in Figure 2.

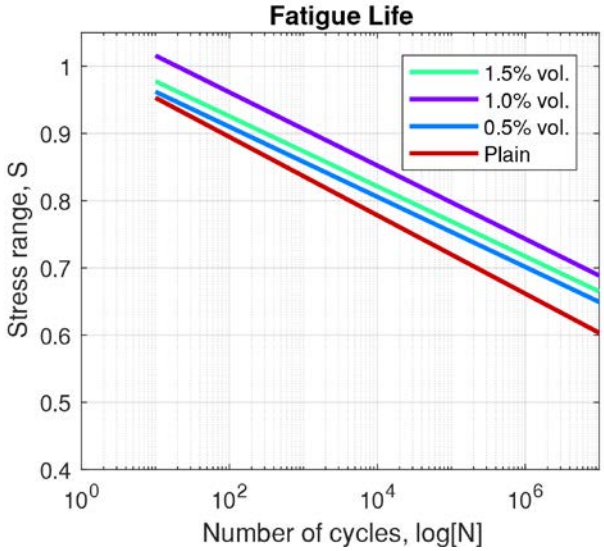

Figure 2. Comparison of the S-N curves for plain concrete and SFRC at various fibre dosages for flexural fatigue.

Based on the regression lines from flexural fatigue tests shown in Figure 2, the effect of fibres seems to be generally positive. The gain in fatigue life is more apparent at lower stress ranges, although it appears overall rather limited and only as long as the fibre dosage remains below 1.5% vol. This could be explained through a double effect of the fibres: on the one hand, fibres bridging micro-cracks can potentially delay their growth and propagation thereby improving the fatigue performance of the concrete. On the other hand, the use of high fibre dosages hinders the workability of the concrete and can result in entrapped air and a greater number of internal voids, which become preferential locations for the initiation of micro-cracks that may lead to fatigue failure.

It is also important to highlight that none of the results reviewed in this study deals with the effect of reverse loading on fatigue life of concrete or FRC. Further studies are therefore required to investigate the impact of varying the stress state of the concrete from tension to compression during cyclic loading, as it may be the case under the application of air-pressure loads, as well as the potentially beneficial effect of fibres.

3 Analysis of temperature and relative humidity

One of the aspects that raised questions during the design of the tunnel lining in previous pre-studies is the temperature variation dictated by the tunnel design guidelines included in the TRVK Tunnel 11 report (see Figure 3). This temperature variation was found critical for the design of the tunnel lining but at the same time it is seen as a rather conservative load case for the local conditions of the tunnel being studied.

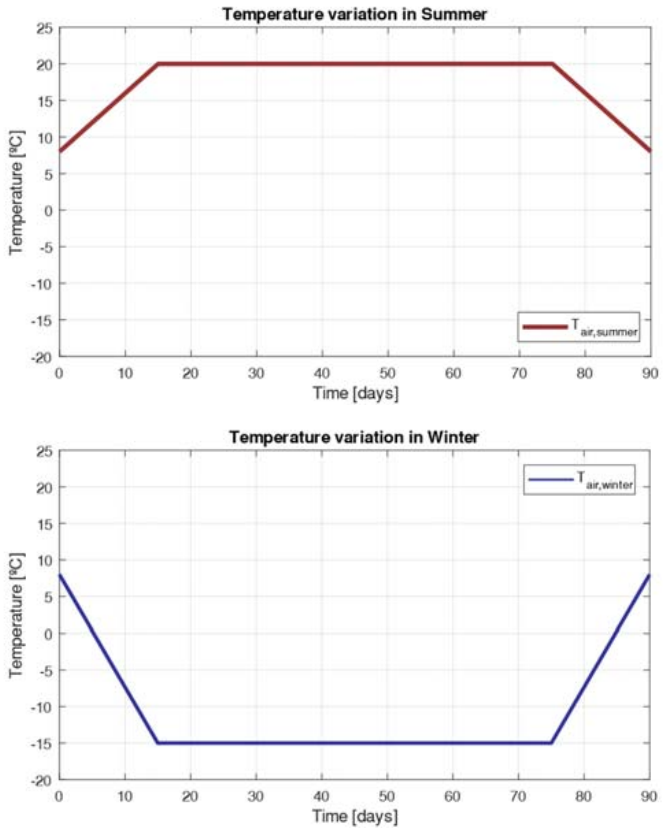

Figure 3. Temperature variation dictated by the tunnel design guidelines included in the TRVK Tunnel 11 report by Trafikverket for summer (top) and winter (bottom).

The aim of this chapter is to determine the average value and yearly variation of the temperature and relative humidity that can be expected inside of a tunnel lining with a length of between 1 to 2 km and located between Göteborg and Borås. These parameters are ultimately used to perform a sensitivity analysis of the effects of restraint cracking induced by temperature changes by comparing the mechanical response of the tunnel subjected to the design temperature and a more realistic temperature variation. Likewise, the relative humidity is used to estimate the risk of restraint cracking stemming from drying shrinkage.

3.1 Study of the temperature

3.1.1 Outdoor air temperature

The first step towards the determination of the temperature inside of the tunnel was to study the temperature variations that can be expected in the air temperature in the region where the tunnel is located. To that end, meteorological data publicly available provided by the SMHI (Sveriges meteorologiska och hydrologiska institut) was downloaded

from: http://opendata-catalog.smhi.se/explore/. In particular, data from two meteorological stations located in the area of interest, one in the airport of Landvetter and the other near the town of Bollebygd, were inspected. The position of the meteorological stations used in this study is depicted in Figure 4.

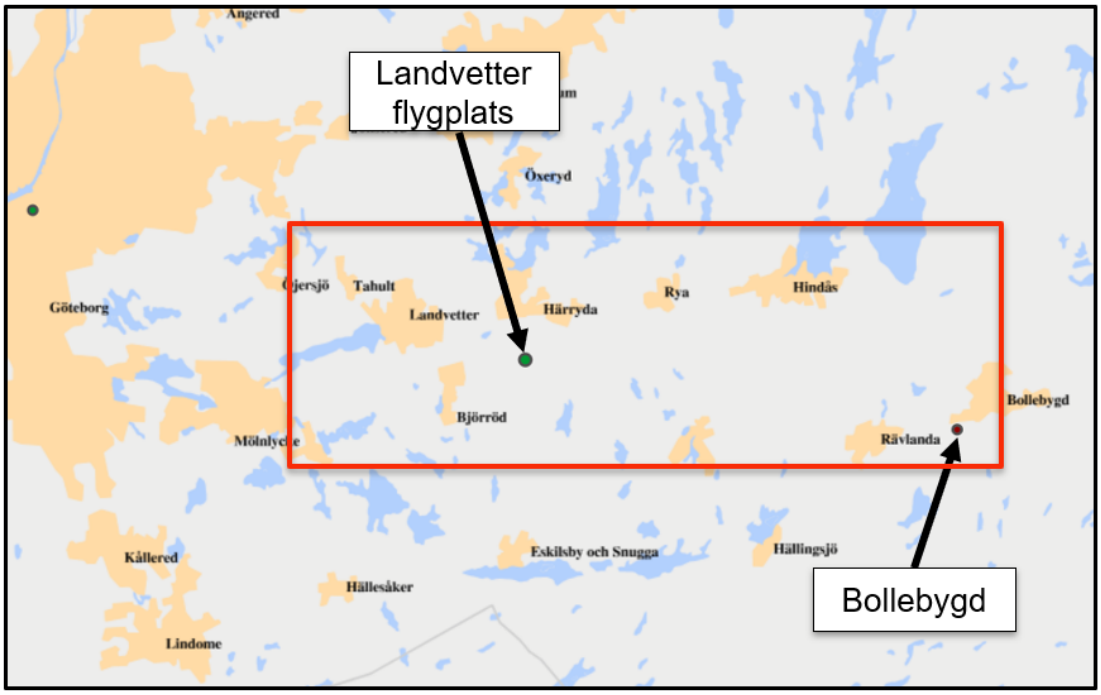

Figure 4. Position of the meteorological stations from where temperature and relative humidity data was retrieved.

From these two stations, the maximum and minimum daily temperatures were extracted for several years in the period 1978 – 2017 for the Landvetter station and in the period 1945 – 1986 for the Bollebygd station. The two sets of temperature data are graphically presented in Figure 5 and Figure 6, respectively, including the average curves for the maximum, minimum and mean temperature. The comparison of these temperature data with the design temperature values shows that indeed the assumption of a 60-day period with a constant temperature of -15ºC does not correspond to the reality, as such low temperature are only reached sporadically and for much shorter periods.

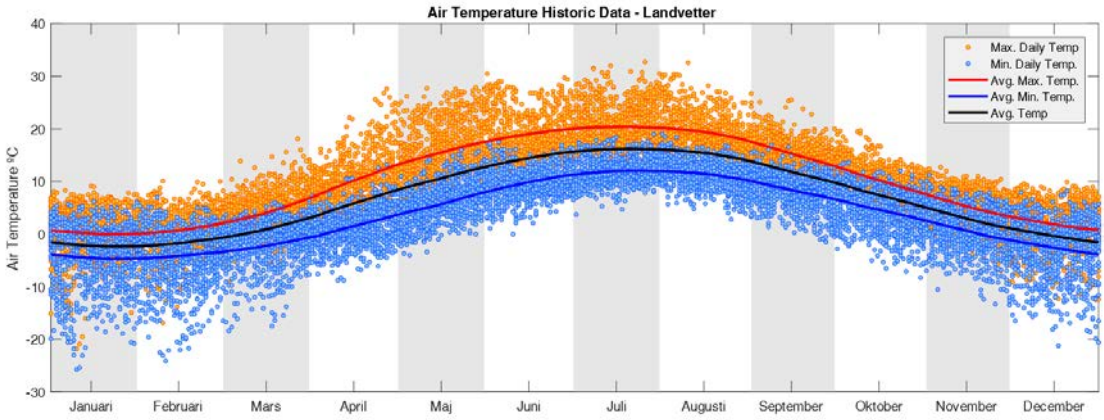

Figure 5. Historic data of the air temperature measured by the meteorological station in Landvetter between 1978 and 2017.

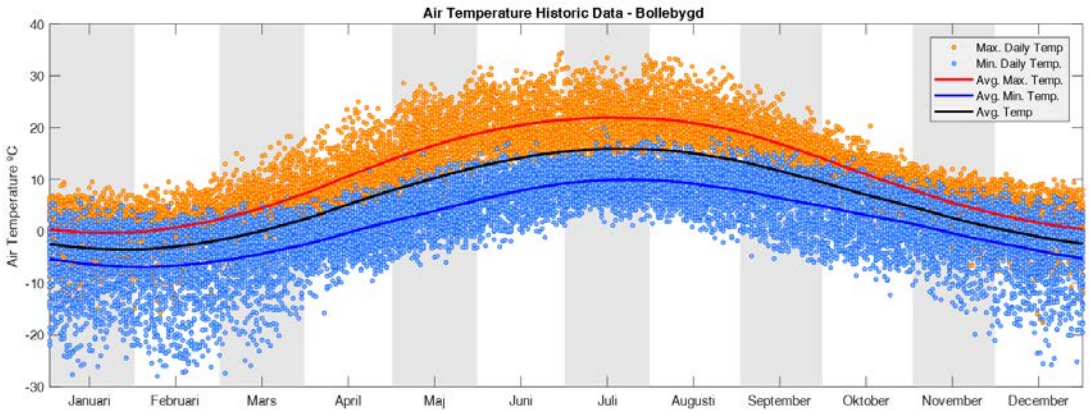

Figure 6. Historic data of the air temperature measured by the meteorological station in Bollebygd between 1945 and 1986.

Since it is stated in the guidelines that the design temperature corresponds to the 50-year return period temperature, a statistical evaluation of the data from the Landvetter station was carried out to obtain a more meaningful comparison. The average temperature over the 60 coldest days of the year was computed for a total of 27 years and the results were fitted to a Generalized Extreme Value probability distribution, which is presented in Figure 7. From the fitting, the temperature with a 2% probability to be exceeded, corresponding to the 50-year return period, was found to be about -7.2ºC. Note that the temperature in the horizontal axis of Figure 7 has opposite sign.

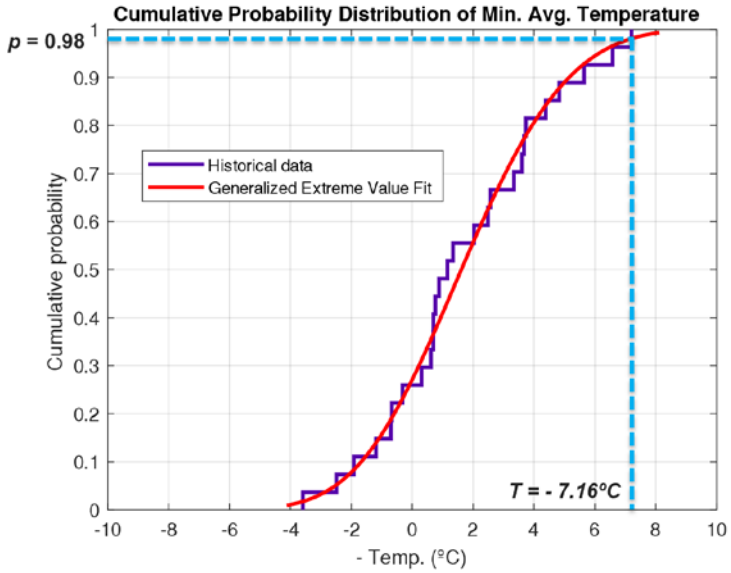

Figure 7. Cumulative probability distribution of the minimum yearly temperature (average over a 60-day period) and Generalized Extreme Value fit curve. The horizontal axis displays the temperature with opposite sign.

3.1.2 Air temperature inside of the tunnel

Once the air temperature outdoors has been obtained from the historic meteorological data, the expected air temperature inside of the tunnel needs to be determined. To do that, real temperature measurements carried out by Trafikverket between October 2009 and May 2010 at the entrance and inside of the Åsatunnel were analyzed. The measured temperatures by Trafikverket are depicted in Figure 8 where the data from the Landvetter during the same period and the yearly average are also included for the sake of comparison.

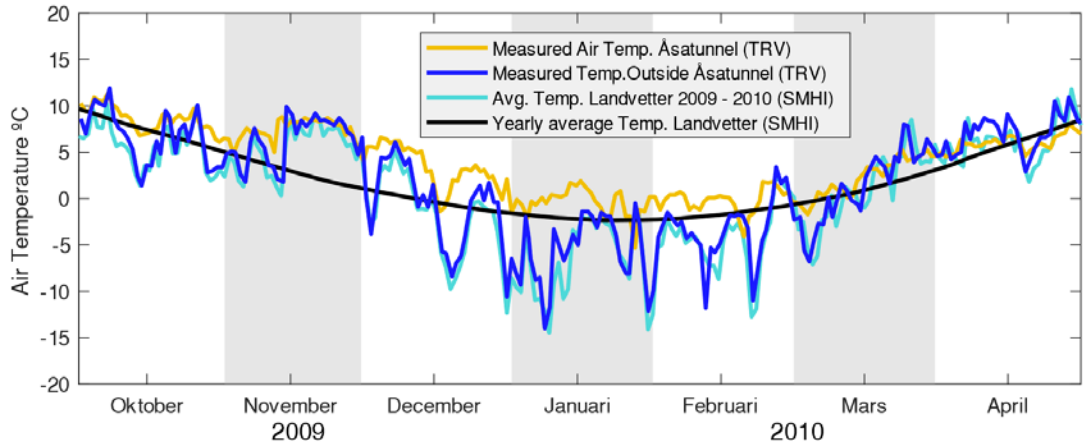

Figure 8. Measurements of the air temperature outside and inside of the Åsatunnel carried out by Trafikverket and comparison with the temperature data from the Landvetter station for the same time period and with the yearly average.

As observed in Figure 8, a very good agreement exists between the outdoor air temperature measured by Trafikverket and at the Landvetter station, indicating temperature variations between the two locations are not significant. Moreover, in comparison with the yearly average temperature, that particular winter seemed colder than the average.

To determine the expected average temperature inside of the tunnel, the following procedure consisting of four steps was applied:

1. The difference between the inside and outside temperature measurements was computed for the Åsatunnel (Figure 9.a).
2. A smooth curve based on a moving average filter is applied to the computed temperature difference (Figure 9.b).
3. The temperature difference for the missing months (summer period) is assumed to follow the same distribution function but with a changed sign (Figure 9.c).
4. The magnitude of the expected temperature difference is reduced to take into account the lower temperatures of the winter during which data was measured (Figure 9.d).

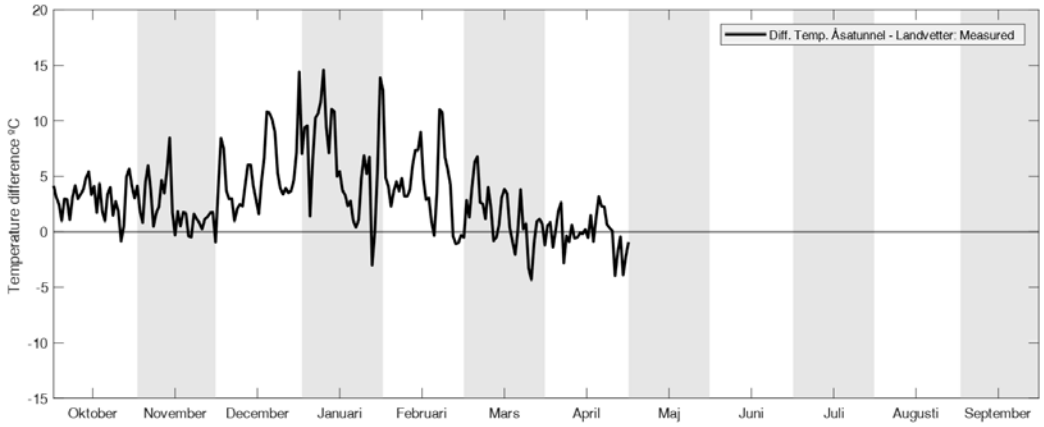

(a)

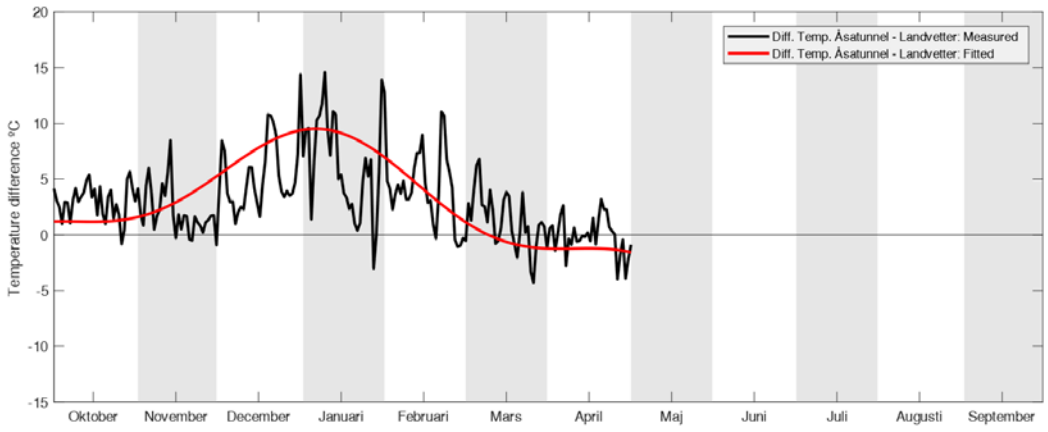

(b)

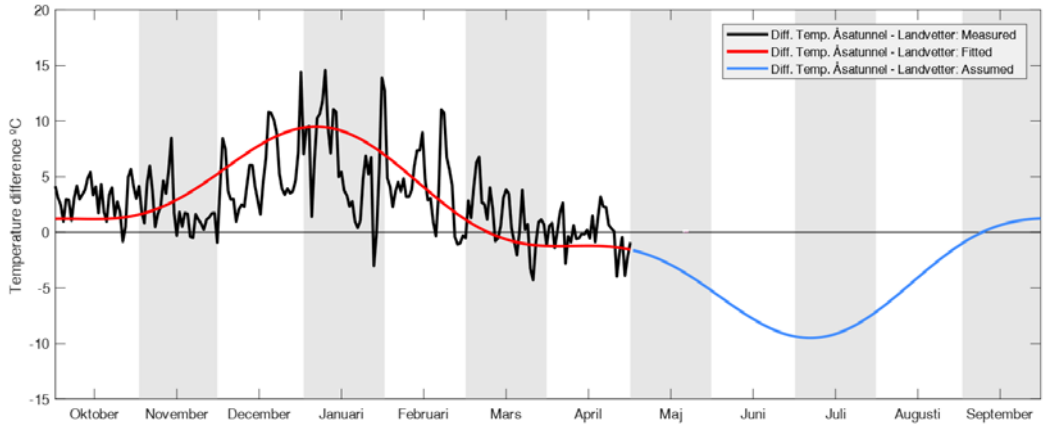

(c)

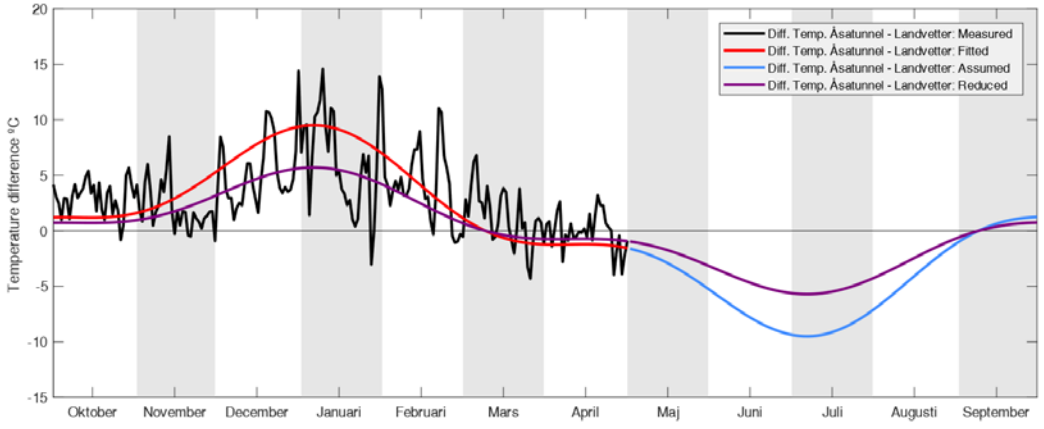

(d)

Figure 9. Procedure followed to determine the expected average temperature difference between the inside and outside of the tunnel based on temperature measurements by Trafikverket in the Åsatunnel.

Subsequently, using the yearly average air temperature outside the tunnel obtained in the previous section and the expected temperature difference between the outside and inside of the tunnel that was just determined, the expected yearly temperature variation inside of the tunnel was calculated. The resulting temperature variation inside of the tunnel, which can be later used to determine the actual temperature of the concrete lining and the rock bedding through a heat transfer analysis, is presented in Figure 10.

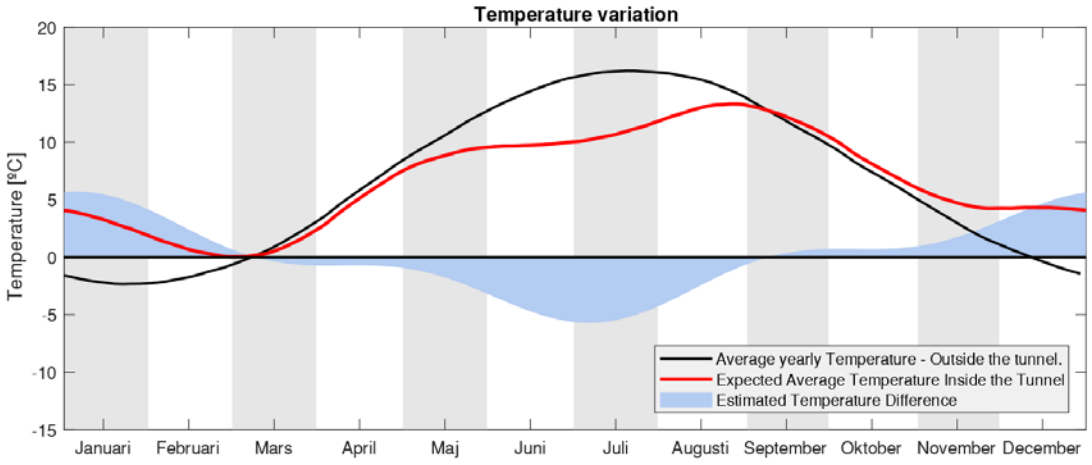

Figure 10. Determination of the expected temperature variation inside of the tunnel (red line) based on historic meteorological temperature measurements (black line) and temperature difference measured between the inside and outside of the Åsatunnel (shaded areas).

3.2 Study of the relative humidity

Similar to what has been shown in Section 3.1 for the temperature, the study of the relative humidity conditions inside of the tunnel was also initiated from the analysis of historic data obtained from the meteorological station of Landvatter. A sample of the daily average relative humidity measured during the period 2013 – 2017 is presented in Figure 11. A general trend is observed where the relative humidity reaches its peak during the months of December and January while the lowest values are found around April – May. The yearly average and a smoother curve resulting from the application of a moving average filter are also presented in Figure 11 as red and blue lines, respectively. The black-dashed line indicates the mean value of the yearly average, which is approximately 82% RH.

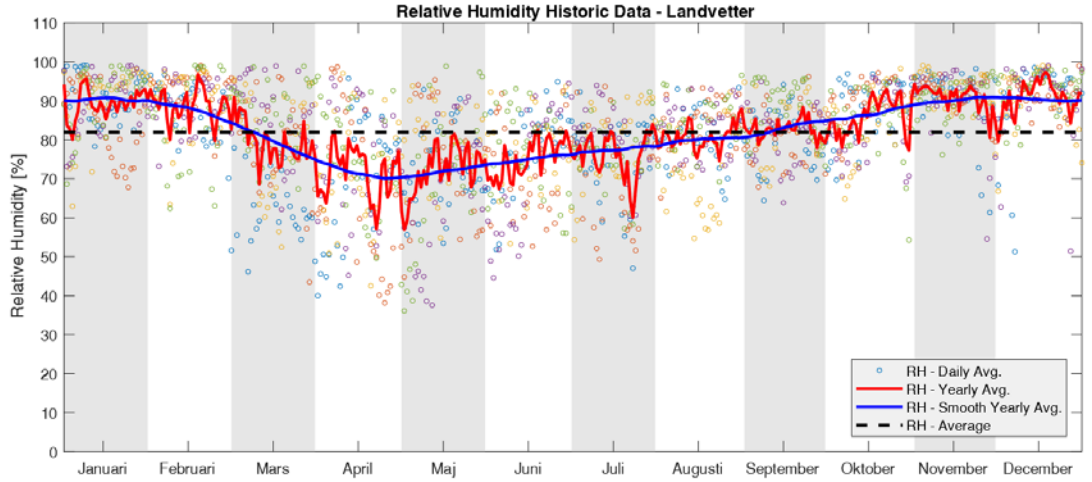

Figure 11. Historic data of the relative humidity measured by the meteorological station in Landvetter between 2013 and 2017.

To estimate the relative humidity inside of the tunnel, the first step involved the calculation of the dew-point, i.e. the saturation vapor content, outside of the tunnel. The dew-point can be expressed as a function of the temperature and the partial vapor pressure according to Equation (1) [22]:

$$v_S = p_s \cdot \frac{M_v}{R \cdot (273.15 + T)} \quad \textbf{(1)}$$

where v_s is the dew-point or saturation vapor content, p_s is the partial vapor pressure, M_v = 18.015 mol is the water vapor molar mass, R = 8.31 J·mol^{-1}·K^{-1} is the ideal gas constant and T is the temperature in Celsius degrees. The partial vapor pressure, p_s is in time a function of the temperature and it can be calculated according to the empirically calibrated expressions described by Equation (2) as:

$$p_s = 288.68 \cdot (1.098 + 0.01T)^{8.02} \qquad 0 \le T \le 30 \quad \textbf{(2.1)}$$

$$p_s = 4.689 \cdot (1.486 + 0.01T)^{12.3} \qquad -20 \le T < 0 \quad \textbf{(2.2)}$$

Once the dew-point is known, the actual water vapor content in the air can be determined taking into account that the relative humidity can be defined as the ratio between the vapor content and the saturation vapor content according to Equation (3):

$$RH = \frac{v}{v_s} \cdot 100 \quad \textbf{(3)}$$

The dew-point inside of the tunnel can be analogously calculated using the estimated yearly temperature inside of the tunnel and considering that water vapor content outside and inside of the tunnel must be in equilibrium, the relative humidity inside of the tunnel can be obtained using Equation (3). This procedure is graphically shown in Figure 12.

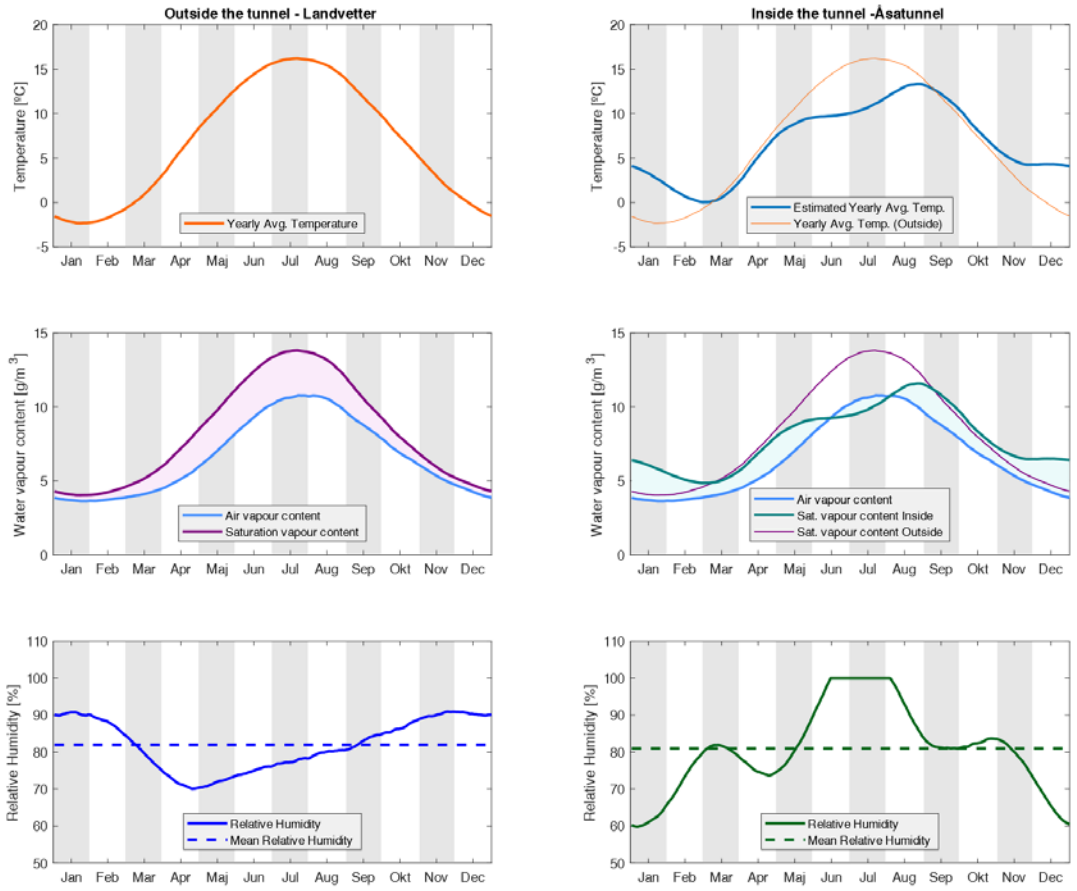

Figure 12. Yearly variation of the air temperature (top row), water vapor content in the air (center row) and relative humidity (bottom row) taken from the meteorological station in Landvetter (left column) and estimated inside of the tunnel (right column).

Due to the difference in temperature, it can be observed from Figure 12 that the variation of the relative humidity inside of the tunnel differs significantly from the variation in relative humidity measured outdoors. To check whether the obtained results are meaningful, a comparison was performed between the estimated variation of the relative humidity in the tunnel under study and relative humidity measurements performed in the railway tunnel of Gevingås (located in central Norway) obtained from [23]. The two curves are presented in Figure 13, where it can be seen that both present clear similarities in terms of the periods of highest and lowest relative humidity as well as the range of relative humidity values, i.e. between approximately 60% and 100% RH. These results can be used to determine the rate of water evaporation at the concrete surface and the subsequent transport of moisture within the concrete, which can then be used to calculate the evolution of drying shrinkage strain of the concrete lining.

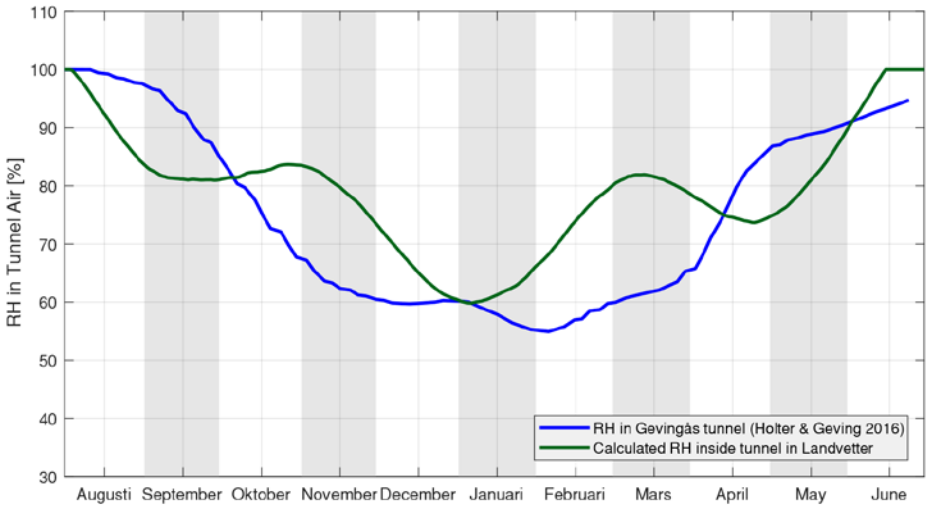

Figure 13. Comparison of the relative humidity variation inside of the tunnel between the calculated values for the tunnel under study and the Gevingås tunnel in central Norway.

4 FE analysis of the tunnel lining

This chapter describes the model used to analyse the structural behaviour of the tunnel lining under the combined action of one or various loads including self-weight, air pressure and suction, non-uniform temperature variations and drying shrinkage. Similarly, the heat transfer and moisture transport models used to convert the results obtained in Chapter 3, i.e. air temperature and relative humidity, into the corresponding inputs for the structural model, i.e. concrete surface temperature and concrete shrinkage strain, are also described.

4.1 Geometry

The geometry of the inner concrete lining represents a reference cross-section of the double-track railway tunnel that was taken from the first pre-study report. The radius of the lining section varies between the vault and the side walls which results in a constant thickness of 300 mm in the vault and a slightly larger variable thickness in the side walls. The geometry of the cross-section is presented in Figure 14.

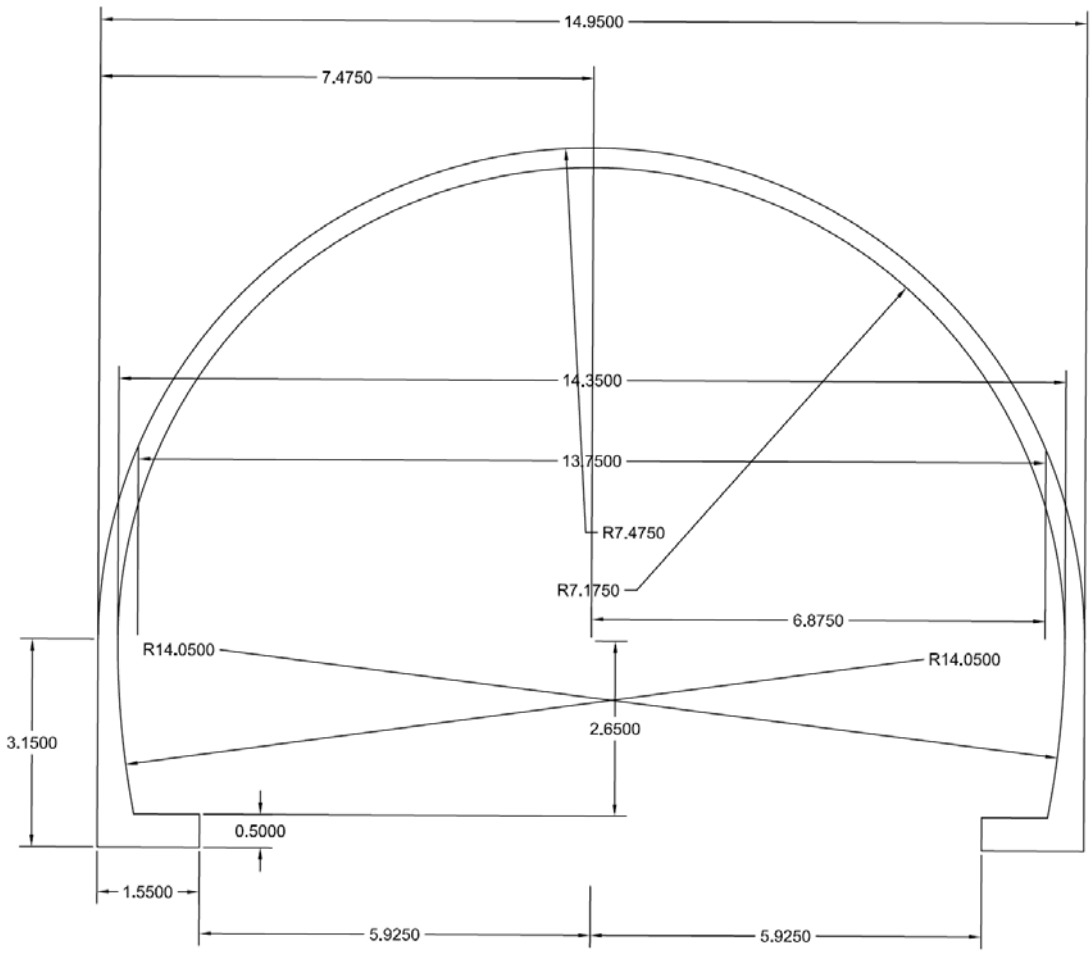

Figure 14. Reference cross-section of the double-track railway tunnel. Measurements are in m.

4.2 Materials

4.2.1 Steel fibre reinforced concrete

The mechanical properties of the steel fibre reinforced concrete used in the lining model were obtained from the first pre-study, which in turn were determined according to the German guidelines for steel fibre reinforced concrete (DAfStb) [3]. As for the crack model, a total strain rotating crack model was used. In the model, cracking initiates once the stresses reach the tensile strength of FRC, which is approximately the same as for plain concrete, cf. [24,25]. Thereafter, crack-bridging stresses will develop the value of which depends on the opening of the crack according to Figure 15. Traction-Separation law describing the post-cracking behaviour of the fibre reinforced concrete used in the finite element analyses. Table 2 summarizes the properties used in the finite element analyses.

Table 2. Mechanical properties of steel fibre reinforced concrete

Linear properties	
Elastic Modulus [GPa]	34
Poisson's ratio [-]	0.2
Mass density [kg/m^3]	2500
Thermal expansion coef. [ºC^{-1}]	10^{-5}
Tensile behaviour	
Uniaxial tensile strength [MPa]	3.2[1)]
Post-cracking tensile behaviour	(see Figure 15)
Crack band width	Based on element size
Compressive behaviour	
Compressive strength [MPa]	43
Compression curve	Ideally plastic

[1)] A smaller tensile strength of 2.56 MPa was used in specific locations to promote crack localization

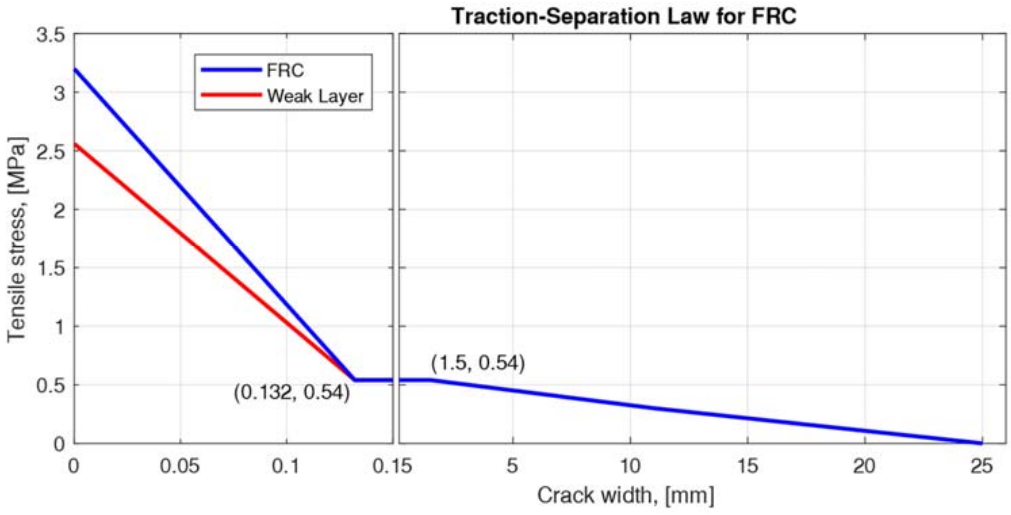

Figure 15. Traction-Separation law describing the post-cracking behaviour of the fibre reinforced concrete used in the finite element analyses.

4.2.2 Rock

The rock bedding has not been explicitly modelled in the structural model of the tunnel lining. Instead, the interaction between the concrete lining and the rock bedding has been simulated as a non-linear contact interface, which is further described in Section 4.4.2. Furthermore, the thermal properties of the rock used for the heat transfer analysis are listed in the Section 4.3.4.

4.3 Loads

4.3.1 Self-weight

The self-weight of the structure is introduced as a body load and is automatically calculated based on the geometry of the structure and the mass density of the material.

4.3.2 Air pressure and suction

The air pressure and suction generated during the passing of the high-speed trains is accounted for as a uniformly distributed load of 8 kPa applied on the entire inner face of the tunnel lining. This value is in accordance to the tunnel design guidelines in the TRVK Tunnel 11 report and has been derived from aerodynamic simulations carried out by the high-speed railway project between Göteborg and Borås.

4.3.3 Non-uniform shrinkage

Differential drying between the exposed surface of the lining and the opposite surface facing the rock, can lead to a non-uniform shrinkage profile in the lining cross-section where the exposed surface has a larger need to shrink. This non-uniform shrinkage will induce a need for curvature and as a result, due to existing restraints, tensile stresses will appear in the inner face, thereby increasing the risk of cracking.

The drying process in the concrete is driven by the transport of moisture towards the exposed surfaces and thus, a moisture transport analysis was performed to estimate the shrinkage profile acting on the tunnel lining. To that end, a 1D model consisting of a single 300 mm segment representing the thickness of the tunnel lining was used. The model was created with the software COMSOL Multiphysics, which allows coupled heat and moisture transport, though in the present analysis the temperature was kept constant at 10ºC. The initial conditions in the concrete were set to a relative humidity of 95%. At the exposed surface, the relative humidity was kept constant at 80% whereas in the other boundary a zero-flux condition was imposed. The hygroscopic material parameters including the moisture storage function, the moisture diffusivity, liquid water permeability and the vapor permeability were adopted according to the EN 15026 as described in [26].

The resulting moisture profile in the concrete after 1 year and after each decade up to a time period of 100 years is shown in Figure 16. As observed, the initial gradient is significant, and it slowly decreases until a nearly uniform relative humidity is reached at the end of the analysis. However, in order to use the results of the moisture transport analysis, the relative humidity profile needs to be translated into drying shrinkage. Even though relatively complex models exist to describe this relationship, a simplified approach as proposed by Gasch et al. [27] was adopted, where the increment of drying shrinkage is assumed proportional to the reduction of relative humidity. In this case, the

proportionality constant was taken so that the final shrinkage, $\varepsilon_{c\infty}$, would yield a value in agreement with the Eurocode 2 [28]. Finally, the non-uniform shrinkage profile corresponding to a 1 year drying period was adopted and discretized into 11 points that were applied in layers to the structural model, as illustrated in Figure 17.

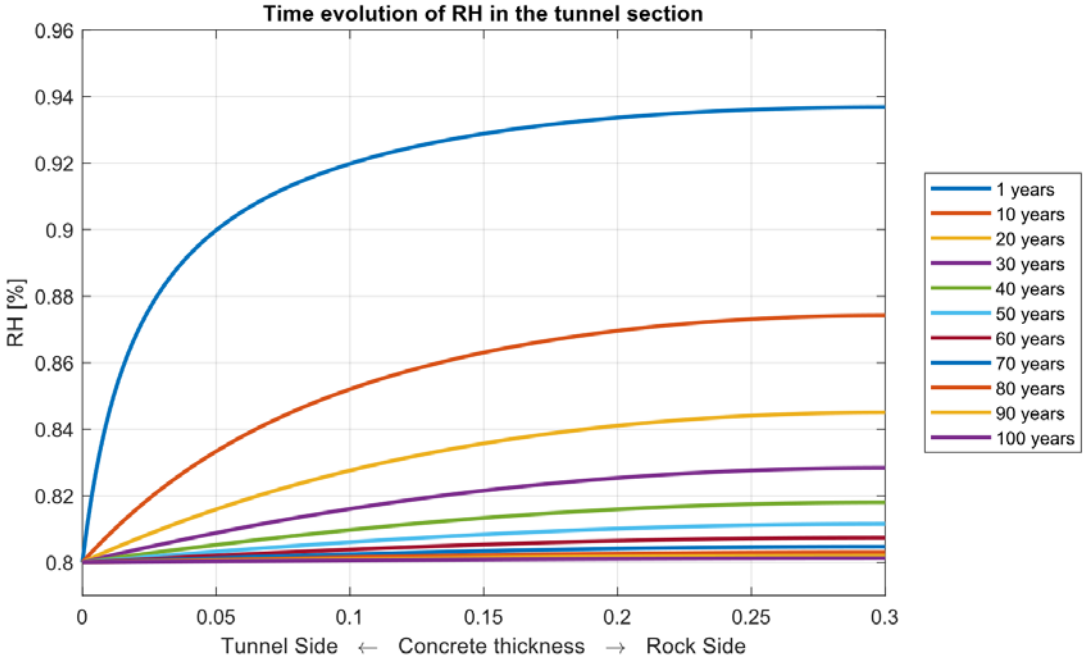

Figure 16. Relative humidity profiles at different time periods obtained from the 1D moisture transport analysis assuming a constant relative humidity at the concrete surface of 80%.

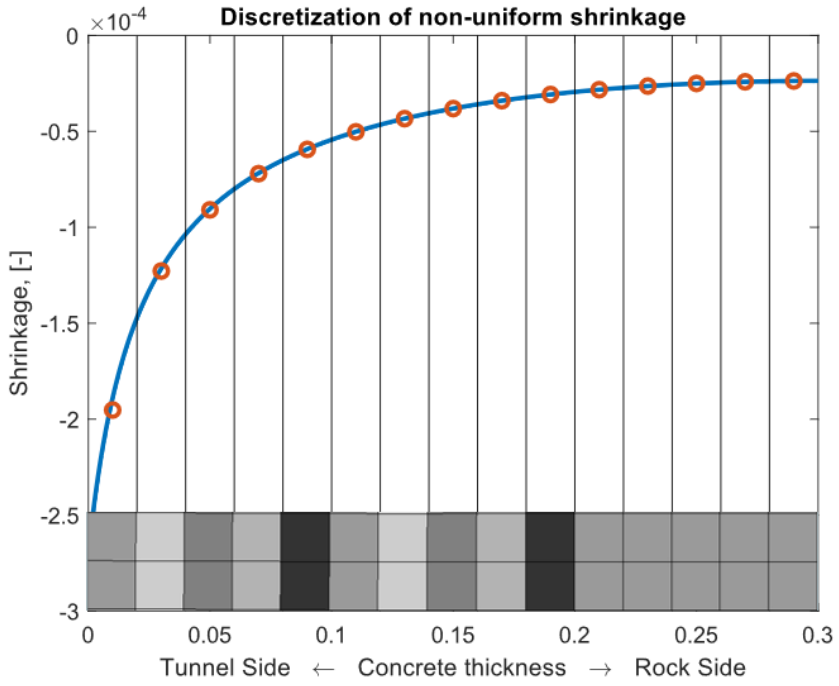

Figure 17. Discretization of the non-uniform shrinkage profile to be applied to the structural model.

4.3.4 Temperature variation

Similar to the effect of drying shrinkage, temperature variations induce stress-independent strains that in the presence of external and/or internal restraints will generate stresses in the concrete. The magnitude of the temperature induced strains depends on the thermal expansion coefficient, which is a material property, and the actual temperature variation in the concrete.

The software used for the structural analysis, DIANA, enables coupled heat transfer and mechanical analysis, thus the temperature and the strains in the concrete section can be computed from the temperature at the boundaries. Thus, unlike in the previous case, it is not necessary to explicitly calculate the strains in the concrete but only the temperature at the external faces of the lining are required.

For the temperature at the surface of the lining, several scenarios were considered. The first, and most conservative, assumed that the temperature of the inner face of the lining was equal to the design temperature (see Figure 3) whereas the outer face remained at a constant temperature of 8ºC. Three more scenarios were considered where the temperature across the tunnel lining was determined through a 1D heat transfer analysis imposing the air temperature inside of the tunnel and the temperature of the rock mass at a far distance from the tunnel, as illustrated in Figure 18. The three scenarios differed in the magnitude of air temperature variation inside of the tunnel which were:

a) The design temperature
b) The yearly average temperature in Landvetter
c) The estimated yearly average temperature inside of the tunnel

All the analyses were performed using the thermal properties for the concrete and rock mass that are presented in Table 3 whereas the heat transfer coefficient used to account for the convection between the air and the concrete was taken as 4.8 W m^{-2} $ºC^{-1}$.

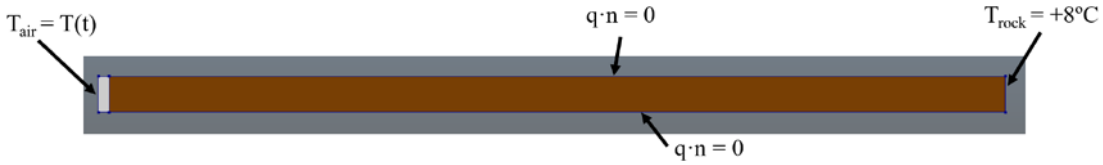

Figure 18. 1D Model for the heat transfer analysis showing the boundary conditions of the model.

Table 3. Thermal properties of the materials used for the heat transfer analysis

Property	Concrete	Rock mass
Thermal conductivity [W m^{-1} $ºC^{-1}$]	1.8	4
Heat capacity [J m^{-3} $ºC^{-1}$]	$2.3 \cdot 10^6$	$2.2 \cdot 10^6$

An example of the temperature distribution across the concrete lining and rock mass obtained from the heat transfer analyses is shown in Figure 19 for the scenario where the air temperature equals the design temperature. As observed, the resulting temperature across the concrete lining shows an almost linear variation whereas an exponential decay of the temperature occurs within the rock mass. From these results, the temperature at the inner and outer faces of the concrete lining can be obtained as a

function of time, which can be later used as the input for the heat transfer-mechanical coupled analysis in the structural model of the tunnel lining. The input for the four different scenarios considered is illustrated in Figure 20.

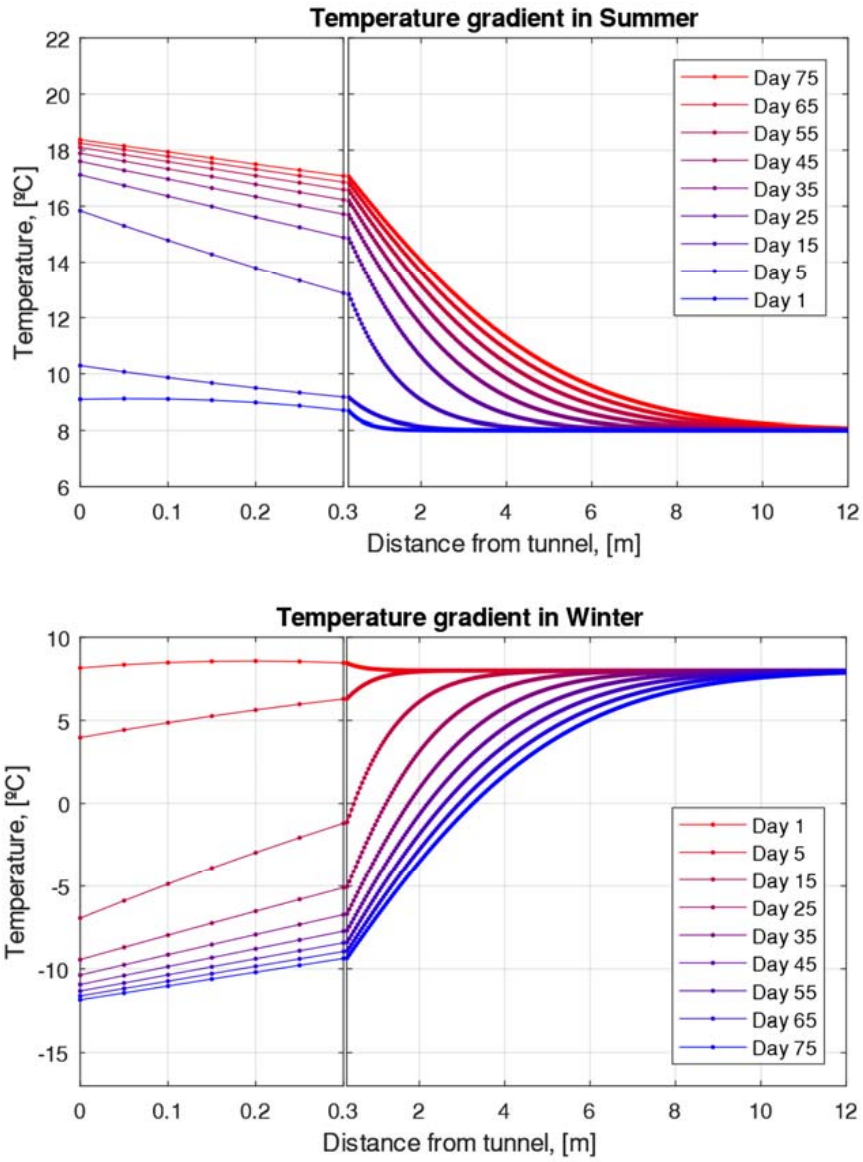

Figure 19. Temperature distribution in the tunnel lining and rock mass obtained from heat transfer analysis considering the design temperature for the summer (top) and winter (bottom).

ΔT = 23 ºC

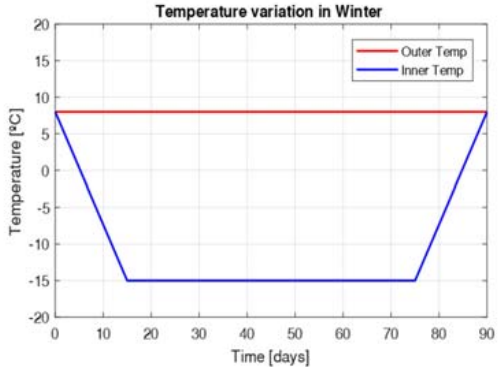

ΔT = 5.8 ºC

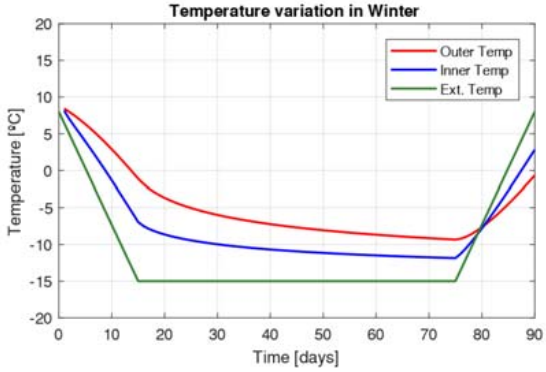

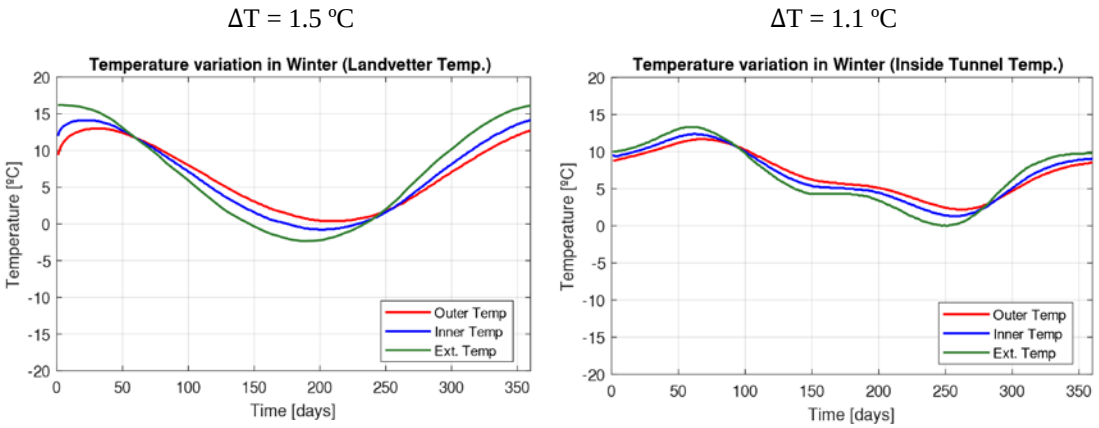

Figure 20. Input temperatures for the heat transfer-mechanical coupled analysis in the structural model of the tunnel lining.

4.4 FE model

For the structural analysis of the tunnel lining a finite element model has been created in the commercial software DIANA 10.2 [29], which allows for the modelling of the material non-linearities of the concrete, such as cracking. The model consists of a one-meter slice of the lining's cross-section.

4.4.1 Mesh

The concrete lining has been modelled using four-node plane stress isoparametric quadrilateral elements with an element size of 20 mm. Moreover, a layer of weak elements with a slightly decreased tensile strength has been introduced at the symmetry axis of the tunnel as well as in the sections where the side walls start increasing their thickness. These sections were critical with regards to bending moments, so the weak layers were introduced to promote crack localization. Figure 21 shows the finite element mesh of the model.

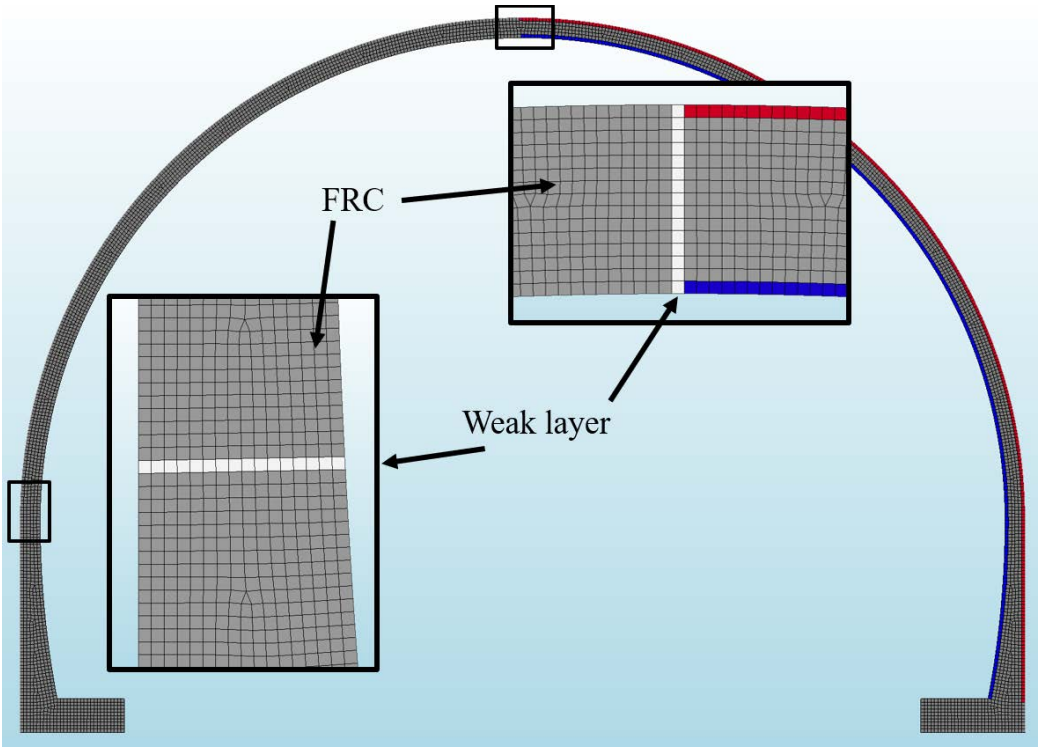

Figure 21. Finite element mesh of the tunnel lining structural model.

4.4.2 Boundary conditions

A set of supports was created at the footings of the tunnel preventing the displacement of the lowest row of nodes in both the vertical and horizontal direction, as shown in Figure 22.

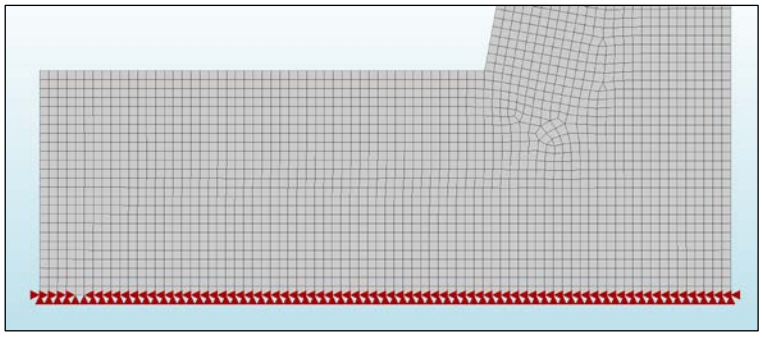

Figure 22. Boundary condition (fixed supports) at the footing of the tunnel.

On the other hand, as previously mentioned, the contact between the concrete lining and the surrounding rock bedding is simulated in the analyses as distributed non-linear springs with contribution only in the normal direction of the tunnel lining, i.e. no shear stresses are introduced between the lining and the rock. However, due to the existence of a drainage layer between the lining and the rock, the stiffness of the springs is decreased to a value of 200 MN/m^3 according to the assumption made in the first pre-study. This is effectively implemented in the present model as an interface layer with the mentioned stiffness in compression and zero stiffness in tension (no tractions). Figure 23 shows the non-linear interface material properties used for the contact interface elements.

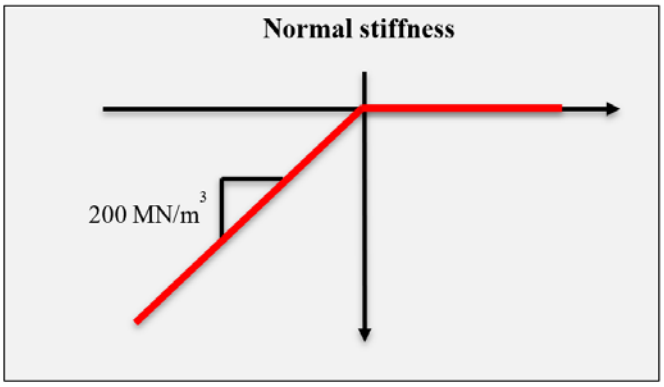

Figure 23. Stiffness properties of the interface elements used to simulate the contact between the concrete lining and the surrounding rock.

An additional non-structural interface layer was added to the inner and outer face of the lining to apply the boundary conditions for the heat transfer coupled analysis, i.e. the temperature that was obtained from the 1D heat transfer analysis in Section 4.3.4.

4.4.3 Analysis

The analysis of the tunnel included several load combinations to study the effect of each individual load as well as to assess their contribution to the overall structural behaviour. The following load combinations are included in this study:

- Self-weight
- Self-weight + Air pressure / Air suction
- Self-weight + non-uniform shrinkage
- Self-weight + temperature variation (4 cases)
- Self-weight + non-uniform shrinkage + temp. variation (case 2) + Air suction

4.5 Results

In this section, the main results from the FE analyses are presented. The results include the variation of stresses along the outermost and innermost element rows of the tunnel lining, which are displayed for half of the tunnel starting from the highest point of the lining and as a function of the lining arc length, see Figure 24. The stress results are complemented with the deformed shape of the tunnel and details of the crack width and sectional stress distribution in cracked sections.

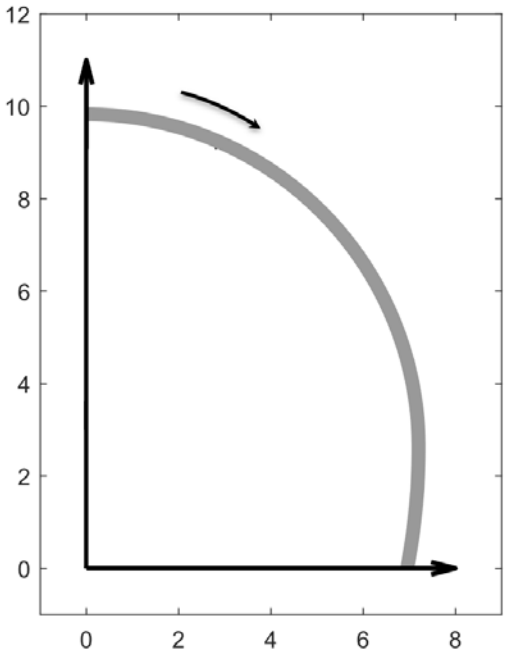

Figure 24. Sketch showing the correct interpretation of the tunnel distance in plots with stress results.

4.5.1 Self-weight

The resulting stresses in the lining due to the application of the self-weight are presented in Figure 25. As observed, a minor bending moment appears in the symmetry plane of the concrete lining which gives rise to extremely small tensile stresses in the inner side of the section. Nevertheless, as we move away from the top of the vault and into the side walls, the concrete lining is subjected to compressive stresses in its entire section. It should be noted that values on the y-axis in Figure 25 are in kPa.

Figure 25. Calculated stresses at the inner and outer face of the concrete lining due to self-weight.

4.5.2 Self-weight + Air pressure / Air suction

The resulting stresses in the lining due to the combined application of the self-weight and either air suction or air pressure, are presented in Figure 26(a) and Figure 26(b), respectively. As observed, the application of a uniformly distributed suction load on the inner face of the lining results in a slight increase of the maximum bending moment in the mid-section of the tunnel while the it simultaneously increases the axial compression load in the lining, thereby completely removing the tensile stresses from all the lining sections.

On the other hand, the application of a uniform pressure from the inside yields the exact opposite results, i.e. the tensile stresses in the mid-section were increased but the compressive axial load was overall reduced, and the maximum bending moment was also decreased.

Since the air pressure and suction arising from the passing of high-speed trains has a cyclic character, it is necessary to ensure that no fatigue problems may arise. For that, we need to look at maximum tensile stress variation in the lining, rather than to the maximum absolute value. Comparing the results in Figure 26, it can be clearly observed that the largest stress variation occurs at the mid-section going from about +180 kPa during the application of internal pressure to about -70 kPa when suction is applied. This means that the air pressure from the passing trains generates a stress range of approximately 250 kPa (0.25 MPa), which is equivalent to roughly 10% of the tensile strength of the concrete.

To check the risk of fatigue, the stress range determined is compared in Figure 27 to the fatigue curves obtained from the literature study. As observed, for 10^6 load cycles, i.e. 10^6 passing trains, the average stress range that can be resisted is above 60% of the concrete tensile strength. Consequently, a stress range of merely 10% of the concrete tensile strength does not entail risk for fatigue problems.

(a)

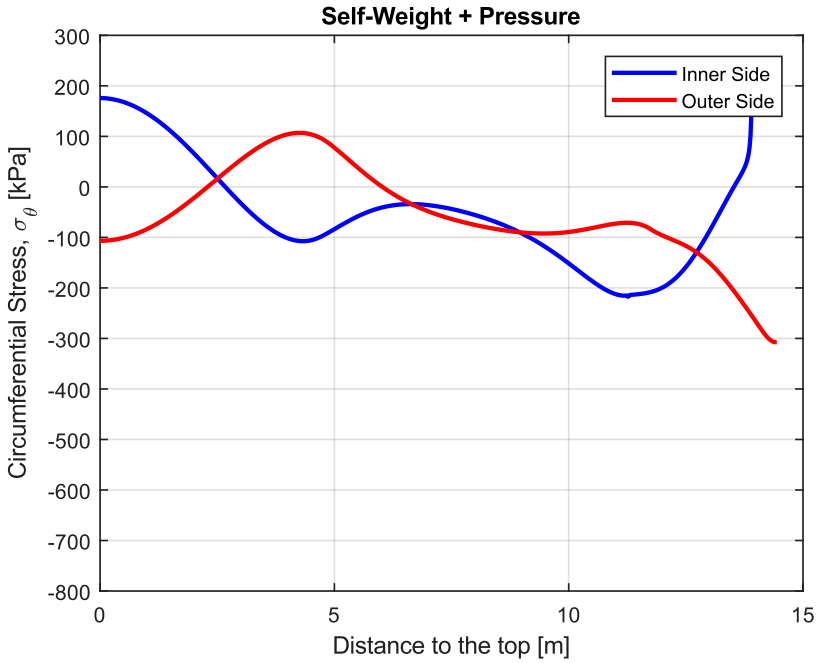

(b)

Figure 26. Calculated stresses at the inner and outer face of the concrete lining due to combined action of self-weight and (a) air suction and (b) air pressure.

It should be noted, however, that the absence of fatigue problems is conditioned to two important aspects: (i) the concrete is assumed uncracked and (ii) no reverse loading occurs, i.e. the maximum stress in the lining does not vary between tension and compression. As previously mentioned, the available information regarding the fatigue behaviour of FRC under these circumstances is not sufficient to ascertain the potential impact of those two scenarios, even though a negative effect can be foreseen.

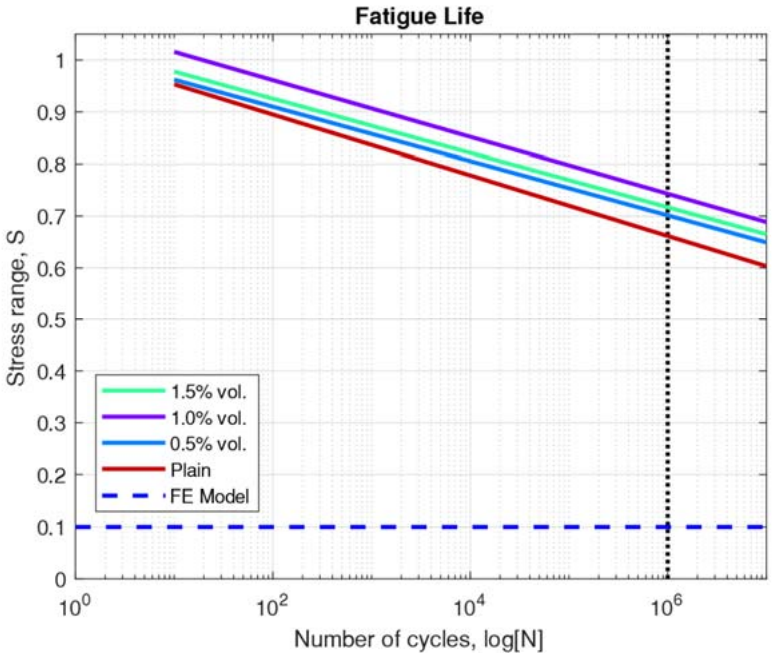

Figure 27. Comparison of the stress range determined from the FE model to the average fatigue life curves obtained from the literature study for various fibre dosages.

4.5.3 Self-weight + non-uniform shrinkage

As shown in Figure 28, the application of a non-uniform shrinkage profile caused the opening of a gap between the tunnel lining and the rock mass of about 2 mm at the highest point of the concrete lining. Moreover, the induced bending moments arising from the internal restraint of the concrete lining caused a crack to form at the mid-section of the tunnel.

A detail of the tunnel showing a zoomed area of the cracked region and displaying the crack width results of the model is shown in Figure 29 together with a diagram presenting the stress distribution in the cracked section, where the height of the crack can be also observed. It can be seen from Figure 29 that formed crack has a very limited crack width of only 0.01 mm and a crack height that is about 10% of the total section. Consequently, drying shrinkage is not considered as a limiting parameter for the design of the tunnel lining since its effects can be minimized through the utilization of shrinkage reducing admixtures or by covering the concrete surface to limit water evaporation.

4.5.4 Self-weight + temperature variation

The effect of the temperature variation was previously identified as one of the critical aspects for the design of the tunnel lining due to the strict design temperature specified in the tunnel design guidelines. In this study, the effect of four different temperature variations have been investigated (see Figure 20):

Case 1: Concrete temperature is the design temperature variation ($\Delta T = 23^{o}C$)

Case 2: Air temperature is the design temperature variation ($\Delta T = 5.8^{o}C$)

Case 3: Air temperature is Landvetter's temperature variation (($\Delta T = 1.5^{o}C$)

Case 4: Air temperature is the estimated temperature variation in the tunnel ($\Delta T = 1.1^{o}C$)

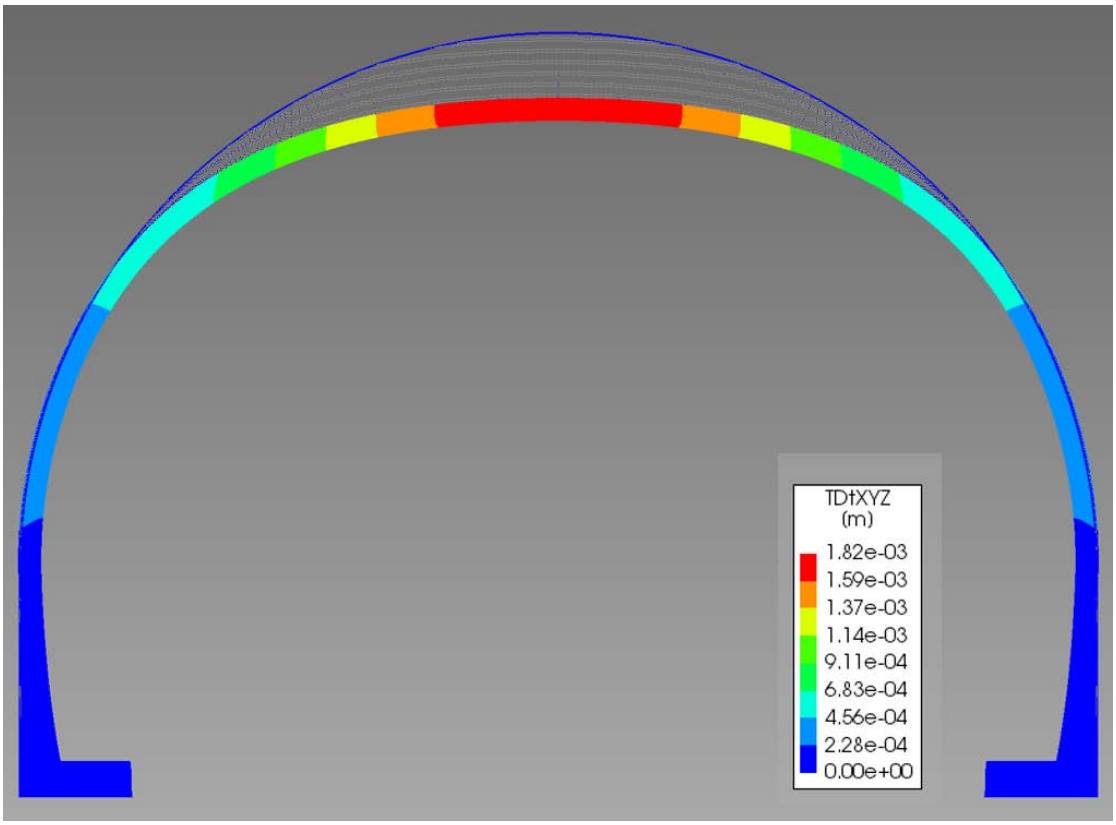

Figure 28. Deformed shape of the tunnel lining under the action of the self-weight and non-uniform shrinkage

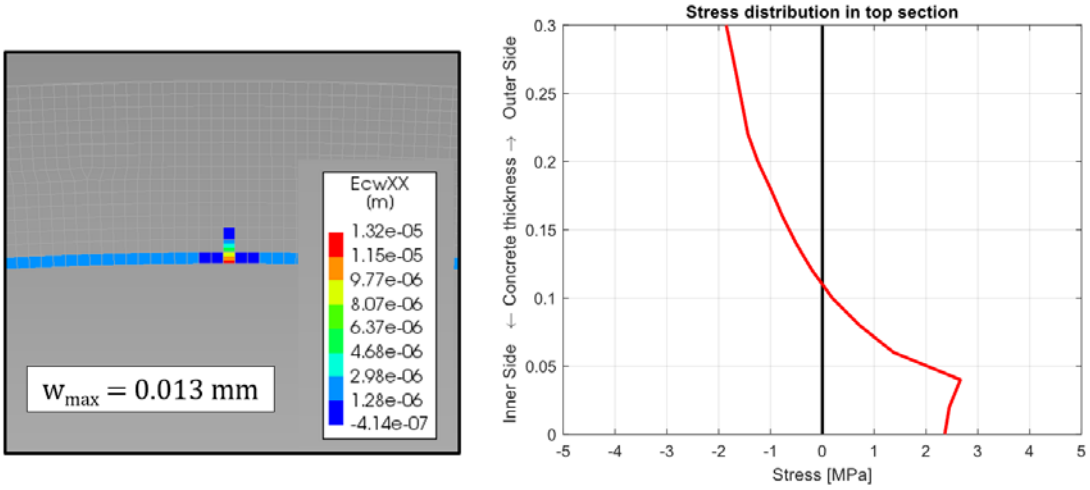

Figure 29. Crack width results from the FE model (left) and stress distribution in the cracked section (right) for the load case of self-weight and non-uniform shrinkage.

In Figure 30, the stress variation along the tunnel lining due to the combined effect of self-weight and temperature variation during the winter period is shown for the four cases considered. Moreover, the subsequent effect of applying the air pressure (dashed lines) and the air suction (dotted lines) is also presented.

The results in Figure 30 show that only Case 1 produces cracking of the concrete lining whereas for the other three cases the tensile stresses remain well below the tensile strength. Moreover, unlike for drying shrinkage, the temperature variation considered in Case 1 results in three fully developed cracks, one at the top-section of the lining and one at each side wall.

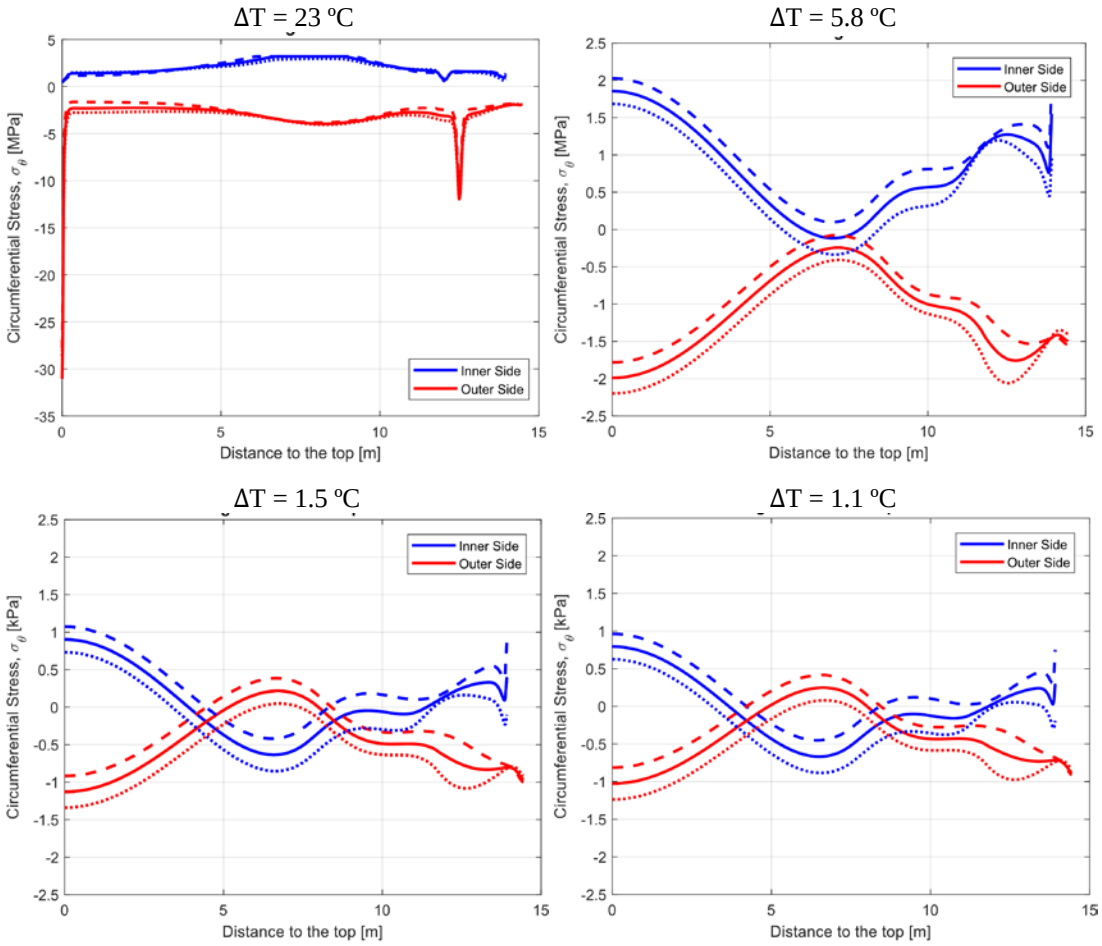

Figure 30. Calculated stresses at the inner and outer face of the concrete lining due to combined action of self-weight and temperature variation (winter) for the four cases considered. The dashed and dotted lines represent the added effect of the air pressure and air suction, respectively.

The deformed shaped of the tunnel lining due to the temperature variation considered in Case 1 is presented in Figure 31, where the three formed cracks can be clearly observed. The maximum deformation of the concrete lining in this case was almost 6 mm, three times larger than for the non-uniform shrinkage load case.

The crack width results obtained from the FE analysis are presented in Figure 32 for the crack formed in the top-section together with the stress distribution. In this case, the crack width reached a maximum value of 1.43 mm in the inner face of the lining, which is much larger than the crack width limitation of 0.3 mm that is often considered in design recommendations with regards to durability, cf. [30]. Similarly, from the stress distribution shown in Figure 32, it can be seen that the crack propagates through most of the lining cross-section, thus resulting in a crack height of about 90% of the lining thickness. This also goes against existing design recommendations for FRC tunnels [2], which indicate that the crack height should not exceed 70% of the element thickness.

The temperature variation applied in Case 1 is, nevertheless, considered as an extreme case which is also unlikely to occur. Even though the temperatures reached inside of the tunnel, or even in the concrete, might be colder than those considered in Cases 2 to 4, a temperature gradient of 23 ºC across the lining thickness would be very difficult to achieve in reality.

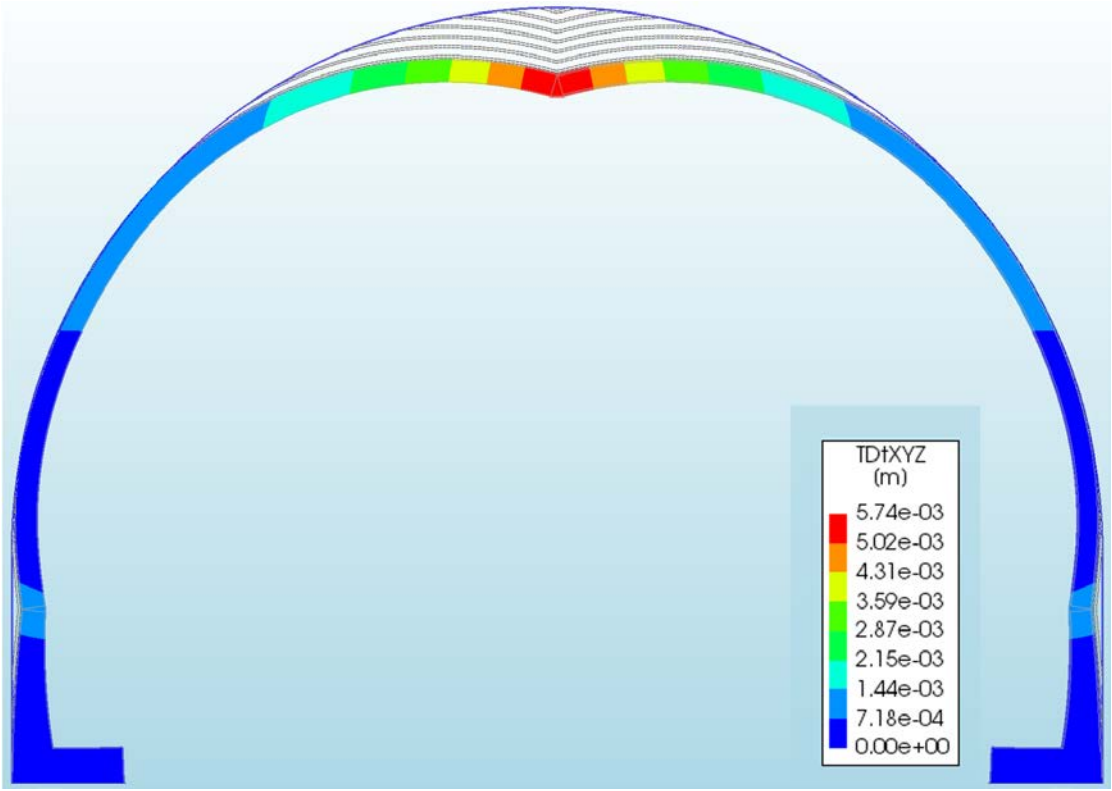

Figure 31. Deformed shape of the tunnel lining under the action of the self-weight and temperature variation Case 1 (winter)

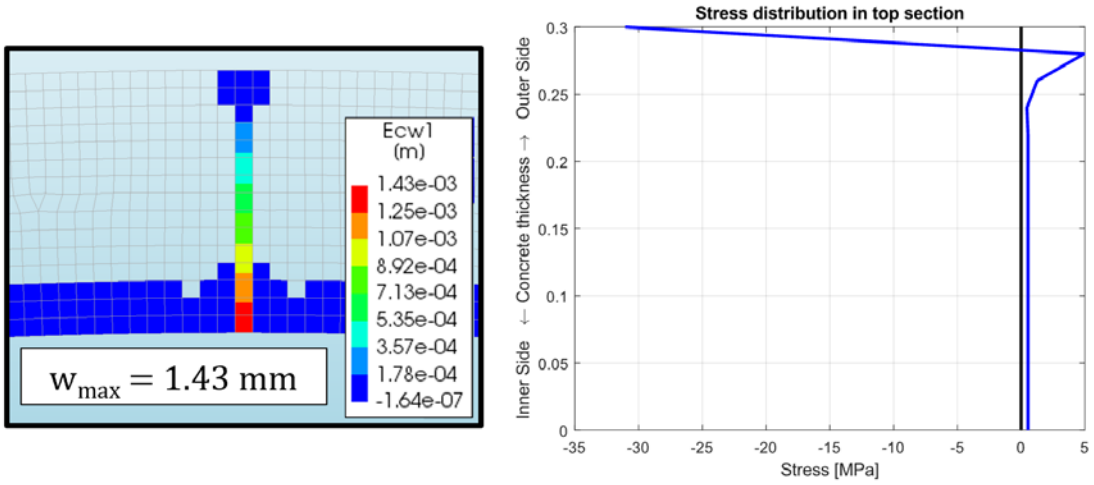

Figure 32. Crack width results from the FE model (left) and stress distribution in the top section crack (right) for the load case of self-weight and temperature variation Case 1 (winter).

On the other hand, uniform variations of the temperature in the concrete lining are not as critical as temperature gradients. This can be clearly seen in Figure 33, where the stresses along the inner and outer face of the tunnel lining are shown for a temperature variation -23 ºC, corresponding to the design temperature, on the entire concrete section. The maximum tensile stress obtained due to a uniform cooling of the tunnel of -23 ºC is about 1.5 MPa whereas it was about 2 MPa for a temperature gradient of only 5.8 ºC (see Figure 30). This indicates that it is in fact the temperature difference across the lining which is the limiting factor for the design.

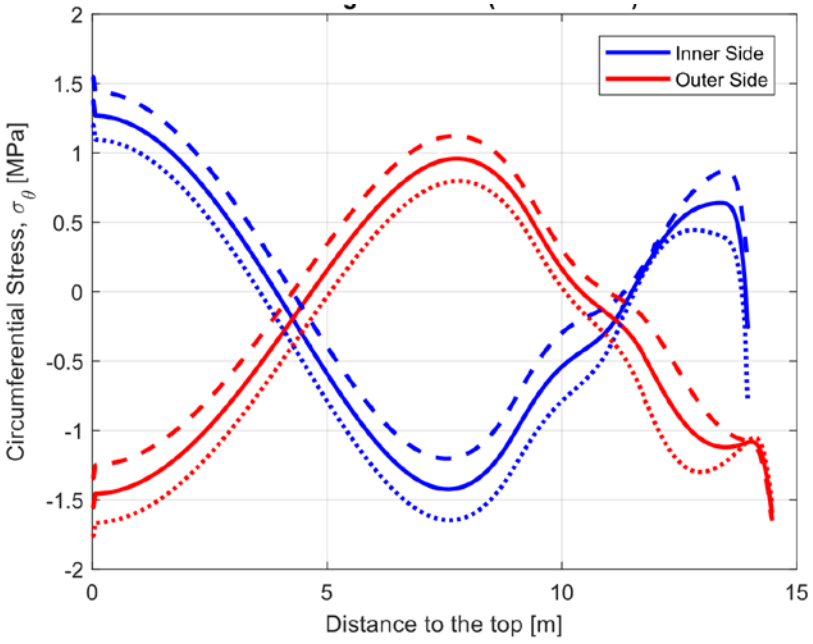

Figure 33. Calculated stresses at the inner and outer face of the concrete lining due to combined action of self-weight and a uniform temperature variation of -23 ºC (no temperature gradient across the lining section). The dashed and dotted lines represent the added effect of the air pressure and air suction, respectively.

Based on the measurements carried out by Trafikverket inside of the Åsatunnel, the difference between the air temperature inside of the tunnel and the temperature of the concrete surface can be expected to be quite low. Even lower is the temperature difference between the concrete surface and the rock. For the particular temperature series shown in Figure 34, the observed difference between the air and concrete temperature is less than 5 ºC during the entire monitored period and the largest temperature differences occur when the air temperature in the tunnel drops suddenly. Therefore, the critical parameters that will control the temperature gradient across the concrete thickness, and consequently the design of the tunnel lining, are the thermal properties of the concrete and how fast the temperature inside of the tunnel changes.

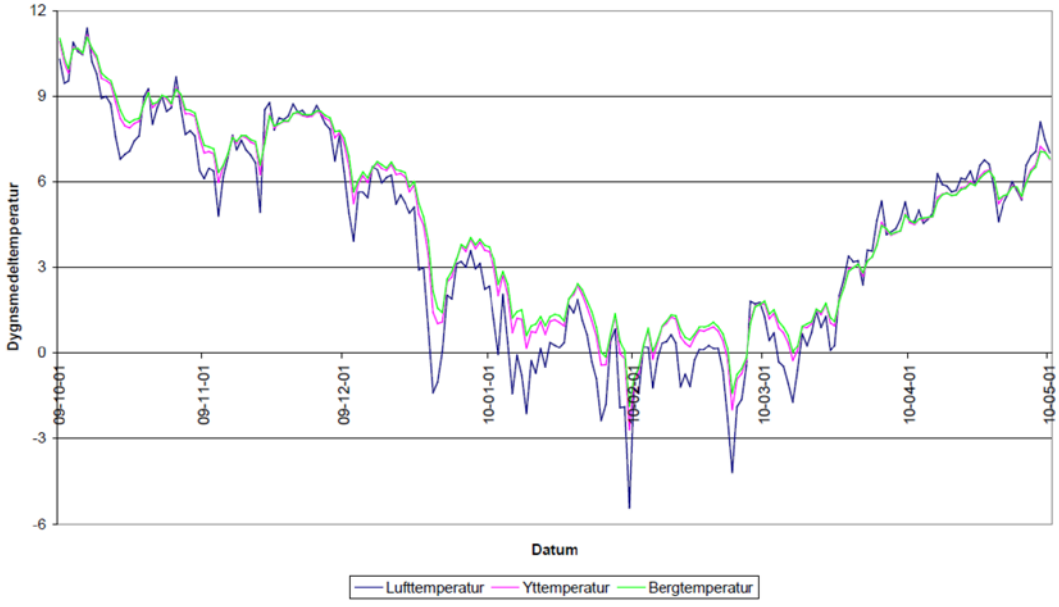

Figure 34. Temperature series monitored inside of the Åsatunnel at different depths (air, concrete surface and rock). The figure is reproduced from data provided by EQUA.

Another important aspect that the FE analysis of the tunnel has also shown is that negative temperature gradients (the air side is colder than the rock side) are far more critical with respect to the risk of cracking than positive gradients. An example of this is shown in Figure 35, where the stress variation along the tunnel lining due to the combined effect of self-weight and temperature variation during the summer period is shown for Case 1 and Case 2. As observed, for a positive gradient of 5.8 ºC, the pressure between the tunnel lining and the rock mass generates a compressive axial force that results in the whole cross-section being in compression. Similarly, even when the positive gradient is increased to 23 ºC, the resulting axial force limits the tensile stresses in the section to only 1 MPa. Nevertheless, it should be noted that this effect will depend on the actual conditions at the interface between the concrete lining and the rock, including the existence of potential gaps, and the true stiffness of intermediate layers such as the drainage layer.

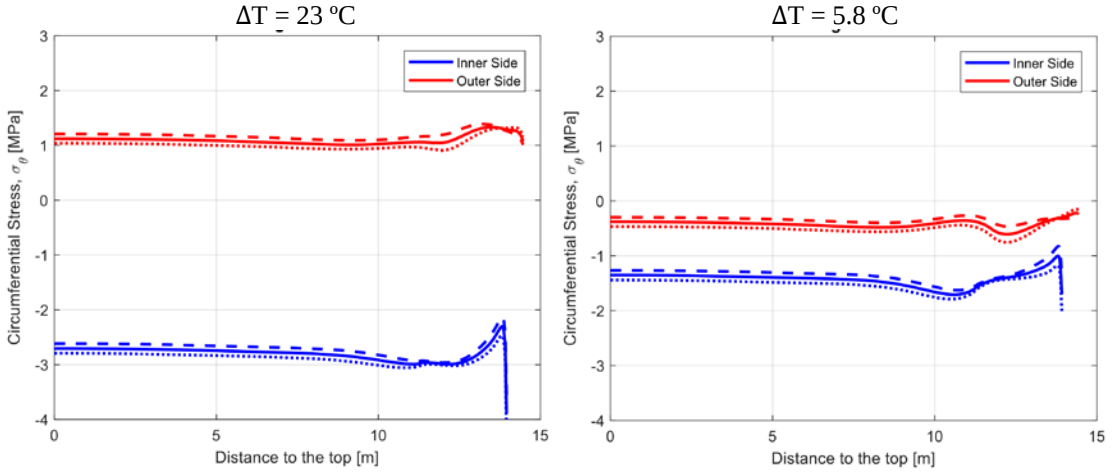

Figure 35. Calculated stresses at the inner and outer face of the concrete lining due to combined action of self-weight and temperature variation (summer) for Case 1 and Case 2. The dashed and dotted lines represent the added effect of the air pressure and air suction, respectively.

4.5.5 Self-weight + shrinkage + temp. variation + Air pressure/suction

In the previous sections it has been shown that: (a) the air pressure and air suction alone have a negligible impact on the uncracked tunnel lining; (b) non-uniform shrinkage might induce cracks, although of minor relevance; and (c) the design temperature is a limiting factor for the design but at the same time it is excessively conservative whereas a more reasonable temperature variation assuming a maximum temperature gradient in the concrete lining of 5.8 ºC will not cause cracking. In this chapter, the effect of combining all these loads sequentially is investigated.

First, the effect of the self-weight and non-uniform shrinkage is computed and then the effect of the temperature variation defined in Case 2 (winter) is added. Before the loads corresponding to the air pressure and suction are included, the model shows that cracking occurs at three locations, analogously as it was shown in Figure 31. However, in this case the cracks exhibit a significantly smaller crack width. Figure 36 illustrates the crack width results obtained from the FE analysis for the crack formed in the top-section together with the stress distribution. As observed, the crack width reached a maximum value only 0.06 mm which is well below the aforementioned 0.3 mm crack width limitation. Similarly, the crack height propagates exactly one third of the lining thickness, which also complies with the previously mentioned tunnel design recommendations.

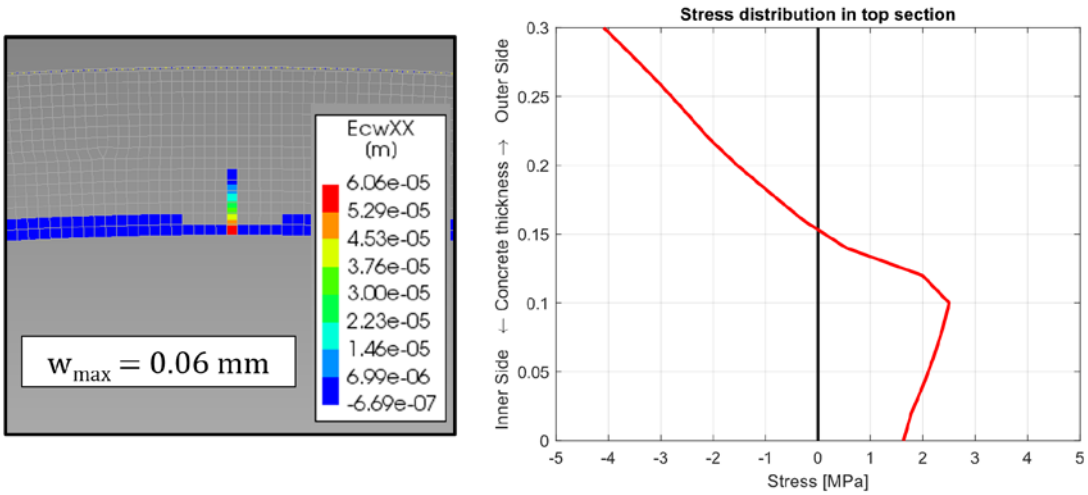

Figure 36. Crack width results from the FE model (left) and stress distribution in the top section crack (right) for the load case of self-weight + non-uniform shrinkage + temperature variation Case 2 (winter).

When adding the loads of air pressure and air suction to the already cracked concrete lining, the resulting effect is completely different from what it was first observed. As shown in Figure 37, the effect of the air pressure in particular causes the existing crack to further open while changing the shape of the stress distribution along the tunnel lining considerably. Moreover, the crack width goes from 0.06 mm to 1.52 mm and the crack height goes from 30% to 90% of the concrete thickness, which renders the cracked section unable to bear any significant loads thereby virtually creating a hinge in the mid-section of the tunnel. Consequently, under the set of loads and assumptions adopted in this pre-study, the results indicate that executing the projected tunnel lining with a FRC mix of the mechanical performance considered is not feasible.

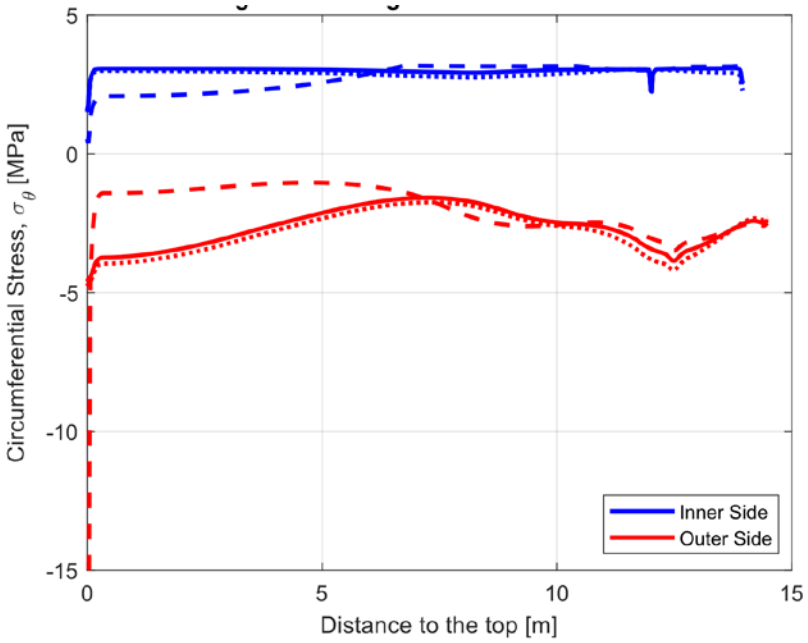

Figure 37. Calculated stresses at the inner and outer face of the concrete lining due to combined action of self-weight, non-uniform shrinkage and the temperature variation defined in Case 2 (winter). The dashed and dotted lines represent the added effect of the air pressure and air suction, respectively.

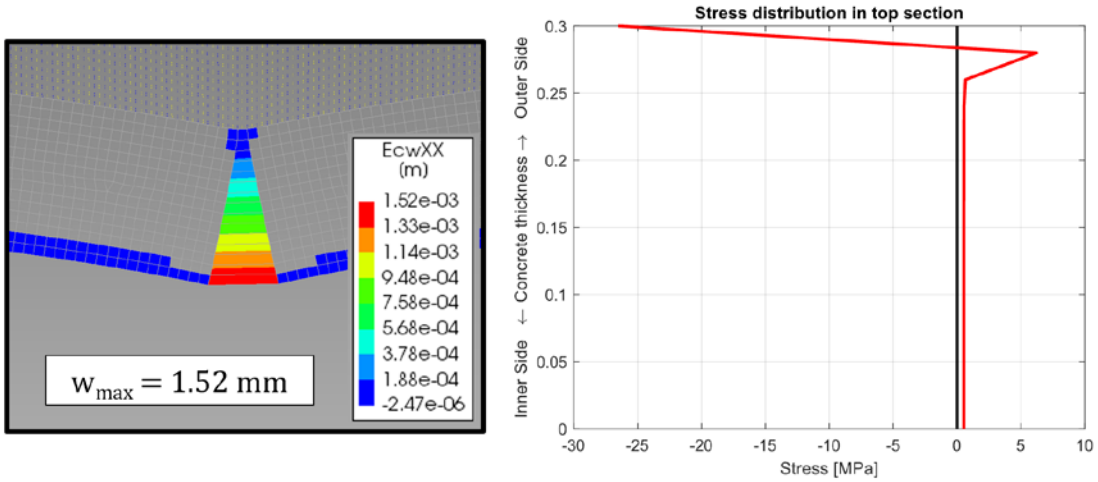

Figure 38. Crack width results from the FE model (left) and stress distribution in the top section crack (right) for the load case of self-weight + non-uniform shrinkage + temperature variation Case 2 (winter) + air pressure.

5 Concluding remarks

5.1 Conclusions of the pre-study

The purpose of this pre-study was to investigate some of the critical aspects that had been previously identified concerning the design of FRC tunnel linings for the high-speed railway project in Sweden. Through a literature review, the collection of environmental data and FE analyses, including heat transfer and mechanical analyses of the tunnel lining, the following conclusions were drawn:

- Despite the absence of design guidelines and standard testing procedures for fatigue of FRC, a significant amount of experimental results have been reported during the last decades. The lack of homogeneity in the specimens and testing conditions across the different studies makes it difficult to establish a direct comparison between the available data to extract conclusive quantitative information. A qualitative assessment of the fatigue behaviour of FRC is nevertheless possible.
- Most of the available experimental results on the fatigue performance of FRC are based on flexural tests. The comparison of the results from several studies showed that fibres can provide a moderate enhancement of the fatigue life for fibre contents of up to 1.0% vol. Thereafter, the introduction of defects in the concrete matrix in the form of small entrapped air voids coming from higher fibre dosages seems to outweigh the beneficial effect of the fibres.
- The review of experimental studies revealed that the vast majority of flexural fatigue results for FRC are based on cyclic loading of uncracked specimens. On the other hand, the results from the only study in which pre-cracked specimens were used indicated that pre-existing cracks may negatively affect the fatigue life. Moreover, no results were found regarding the effect of reverse cyclic loading on the fatigue performance of FRC. Consequently, more experimental research is required to fully understand the fatigue behaviour of FRC under those two particular cases.
- A comparison between the temperature variation dictated by the tunnel design guidelines of Trafikverket and the historic temperature variation measured at various meteorological stations revealed that the design temperature for winter is conservative in terms of both the magnitude of the coldest temperature and its duration.
- The results of a 1D heat transfer analysis as well as the temperature measurements inside of the Åsatunnel indicate that the difference between the air temperature and the temperature at the inner and outer sides of the lining are rather limited. This entails that sub-zero temperatures can be easily reached at the lining-rock interface if the air temperature inside of the tunnel drops below 0 ºC.
- From the structural analysis of the tunnel lining it was found that the action of the air pressure and suction arising from the passing of the high-speed trains resulted in a small stress range of about only 10% of the tensile strength, hence no risk of fatigue problems should be expected. Restraint forces from non-uniform shrinkage were found to induce cracking although very minor.
- Temperature induced cracking was observed to be excessive when using the design temperature, but cracking did not occur when using the temperature variations obtained from the heat transfer analyses. The main aspect governing the cracking of the lining was the existence of negative temperature gradients across the concrete section, which are controlled by factors such as the thermal properties of the concrete, the time-gradient of the air temperature inside of the tunnel or the existence of an insulation layer between the concrete and the rock mass. Uniform temperature

variations and positive gradients have a significantly lower impact on the risk of cracking than negative temperature gradients.

- The action of the air pressure from the trains on a pre-cracked section of the lining resulted in excessively large crack widths with regard to fatigue and durability. Consequently, the current design of the lining is not feasible for the load cases considered.

5.2 Recommendations for crack control

Some measures could be taken to reduce the risk of cracking or to better control its propagation and growth. The following are some examples:

- In order to reduce the risk of cracking due to restraint shrinkage forces, a low shrinkage concrete mix could be designed using shrinkage reducing agents or by applying a diffusion sealing membrane on the inner side of the lining after casting to minimize water evaporation.
- The lining could be executed using a hybrid reinforcement system where FRC would be used in combination with conventional reinforcement bars optimally distributed at certain locations of the lining to better control crack widths locally.

5.3 Suggestions for further research

The work carried out in this pre-study raised some questions that could not be addressed herein and that require further research. Some of these questions are listed in the following:

- The literature review highlighted the current need to further investigate the fatigue behaviour of FRC, particularly with regard to the impact of pre-existing cracks and reverse loading on the fatigue life. These aspects require extensive and carefully planned experimental work.
- Since one of the limiting factors for the design of the tunnel lining in the original design was the temperature gradient across the concrete lining, and the design temperatures were deemed too conservative, it is advised to further study what temperature gradients are expected to occur in reality. This should be carried out by combining detailed numerical simulations and relevant temperature measurements inside existing tunnel linings of the same characteristics.
- One of the methods proposed in previous studies to minimize the tensile stresses in the concrete is to prestress the lining by injecting a cement grouting between the lining and the rock. This method is interesting, and it may potentially work, but its effectivity will depend on various factors that require further investigation. First of all, the long-term effects of concrete, namely creep and shrinkage, will cause the initially induced compressive stress to decrease with time. According to [31], the losses due to creep may amount to up to 40%. Shrinkage could further decrease the initial prestress. Moreover, the presence of cracks in the rock mass might also pose difficulties to achieve the desired pressure behind the lining, since the cement grout may leak through the rock.

References

[1] H. Kawaguchi, Y. Nagasawa, M. Kurita, M. Watanabe, Steel Figer Reinforced Concrete for Extruded Concrete Lining Method, Trans. Japan Concr. Inst. 22 (2000) 229–236.

[2] P. Nanakorn, H. Horii, A fracture-mechanics-based design method for SFRC tunnel linings, Tunn. Undergr. Sp. Technol. 11 (1996) 39–43. doi:10.1016/0886-7798(96)00050-8.

[3] DAfStb - Deutscher Assuchurss für Stahlbeton (German Committee for Structural Concrete), Richtilinie Stahlfaserbeton (Technical rules on steel fibre concrete), Germany, 2010.

[4] Model Code, fib Model Code for Concrete Structures, Wiley-VCH Verlag GmbH & Co. KGaA, Weinheim, Germany, 2010. doi:10.1002/9783433604090.

[5] M.K. Lee, B.I.G. Barr, An overview of the fatigue behaviour of plain and fibre reinforced concrete, Cem. Concr. Compos. 26 (2004) 299–305. doi:10.1016/S0958-9465(02)00139-7.

[6] C.D. Johnston, R.W. Zemp, Flexural Fatigue Performance of Steel Fiber Reinforced Concrete-Influence of Fiber Content , Aspect Ratio , and Type, (1992). doi:10.14359/1875.

[7] F. Germano, G. Tiberti, G. Plizzari, Post-peak fatigue performance of steel fiber reinforced concrete under flexure, Mater. Struct. Constr. 49 (2016) 4229–4245. doi:10.1617/s11527-015-0783-3.

[8] Trafikverket, TRVK Tunnel 11 - Trafikverkets tekniska krav Tunnel, Borlänge, Sweden, 2011.

[9] G. Batson, C. Ball, L. Bailey, E. Landers, J. Hooks, Flexural Fatigue Strength of Steel Fiber Reinforced Concrete Beams, ACI J. 69 (1972) 673–677.

[10] D.E. Otter, A.E. Naaman, Properties of Steel Fiber Reinforced Concrete Under Cyclic Loading., ACI Mater. J. 85 (1988) 254–261. doi:10.14359/2116.

[11] A. Nanni, Fatigue behaviour of steel fiber reinforced concrete, Cem. Concr. Compos. 13 (1991) 239–245. doi:10.1016/0958-9465(91)90029-H.

[12] M. Grzybowski, C. Meyer, Damage accumulation in concrete with and without fiber reinforcement, ACI Mater J. 90 (1993) 594–604. doi:10.14359/4438.

[13] D. Il Chang, W.K. Chai, Flexural fracture and fatigue behavior of steel-fiber-reinforced concrete structures, Nucl. Eng. Des. 156 (1995) 201–207. doi:10.1016/0029-5493(94)00946-V.

[14] C. Huang, G. Zhao, Properties of steel fibre reinforced concrete containing larger coarse aggregate, Cem. Concr. Compos. 17 (1995) 199–206. doi:10.1016/0958-9465(95)00012-2.

[15] T. Mailhot, B. Bissonnette, F. Saucier, M. Pigeon, Flexural fatigue behavior of steel fibre reinforced concrete before and after cracking, Mater. Struct. 34 (2001) 351–359. doi:10.1007/BF02486486.

[16] S.P. Singh, S.K. Kaushik, Flexural Fatigue Analysis of Steel Fiber-Reinforced Concrete, ACI Mater. J. 98 (2001) 306–312.

[17] S.P. Singh, Y. Mohammadi, S.K. Kaushik, Flexural fatigue analysis of steel fibrous concrete containing mixed fibers, ACI Mater. J. 102 (2005) 438–444. doi:10.1631/jzus.2006.A1329.

[18] A.G. Graeff, K. Pilakoutas, K. Neocleous, M.V.N.N. Peres, Fatigue resistance and cracking mechanism of concrete pavements reinforced with recycled steel fibres recovered from post-consumer tyres, Eng. Struct. 45 (2012) 385–395. doi:10.1016/j.engstruct.2012.06.030.

[19] S. Goel, S.P. Singh, Fatigue performance of plain and steel fibre reinforced self compacting concrete using S-N relationship, Eng. Struct. 74 (2014) 65–73. doi:10.1016/j.engstruct.2014.05.010.

[20] N.K. Banjara, K. Ramanjaneyulu, S. Sasmal, V. Srinivas, Flexural Fatigue Performance of Plain and Fibre Reinforced Concrete, Trans. Indian Inst. Met. 69 (2016) 373–377. doi:10.1007/s12666-015-0770-y.

[21] B. Isojeh, M. El-Zeghayar, F.J. Vecchio, Fatigue Behavior of Steel Fiber Concrete in Direct Tension, J. Mater. Civ. Eng. 29 (2017) 04017130. doi:10.1061/(ASCE)MT.1943-5533.0001949.

[22] L.E. Nevander, B. Elmarsson, Fukt handbok - praktik och teori, third edit, AB Svensk Byggtjänst och författarna, 1994.

[23] K.G. Holter, S. Geving, Moisture Transport Through Sprayed Concrete Tunnel Linings, Rock Mech. Rock Eng. 49 (2016) 243–272. doi:10.1007/s00603-015-0730-1.

[24] G. Tiberti, F. Germano, A. Mudadu, G.A. Plizzari, An overview of the flexural post-cracking behavior of steel fiber reinforced concrete, Struct. Concr. 19 (2018) 695–718. doi:10.1002/suco.201700068.

[25] I. Löfgren, Fibre-reinforced concrete for industrial construction - a fracture mechanics approach to material testing and structural analysis, Chalmers University of Technology, 2005.

[26] COMSOL Multiphysics, Heat and Moisture Transport in a Semi-Infinite Wall, (n.d.). https://www.comsol.com/model/download/470381/models.heat.semi_infinite_wall.pdf .

[27] T. Gasch, R. Malm, A. Ansell, A coupled hygro-thermo-mechanical model for concrete subjected to variable environmental conditions, Int. J. Solids Struct. 91 (2016) 143–156. doi:10.1016/j.ijsolstr.2016.03.004.

[28] EN 1992-1-1 Eurocode 2, EN 1992-1-1 Eurocode 2: Design of concrete structures - Part 1-1: General rules and rules for buildings, (2004).

[29] TNO Diana, Finite Element Analysis, Diana User's Manual 9.6, (2015).

[30] V. Marcos-Meson, A. Michel, A. Solgaard, G. Fischer, C. Edvardsen, T.L. Skovhus, Corrosion resistance of steel fibre reinforced concrete - A literature review, Cem. Concr. Res. 103 (2018) 1–20. doi:10.1016/j.cemconres.2017.05.016.

[31] Y. Simanjuntak, M. Marence, A.E. Mynnet, A.J. Schleiss, Mechanical-hydraulic interaction in the cracking process of pressure tunnel linings, Int. J. Hydropower Dams. 20 (2013) 112–119.